ALFRED-WEGENER-INSTITUT
HELMHOLTZ-ZENTRUM FÜR POLAR- UND MEERESFORSCHUNG

724
2018

Berichte
zur Polar- und Meeresforschung

Reports on Polar and Marine Research

The Expedition PS113 of the Research Vessel POLARSTERN to the Atlantic Ocean in 2018

Edited by

Volker Strass

with contributions of the participants

HELMHOLTZ GEMEINSCHAFT

Die Berichte zur Polar- und Meeresforschung werden vom Alfred-Wegener-Institut, Helmholtz-Zentrum für Polar- und Meeresforschung (AWI) in Bremerhaven, Deutschland, in Fortsetzung der vormaligen Berichte zur Polarforschung herausgegeben. Sie erscheinen in unregelmäßiger Abfolge.

Die Berichte zur Polar- und Meeresforschung enthalten Darstellungen und Ergebnisse der vom AWI selbst oder mit seiner Unterstützung durchgeführten Forschungsarbeiten in den Polargebieten und in den Meeren.

Die Publikationen umfassen Expeditionsberichte der vom AWI betriebenen Schiffe, Flugzeuge und Stationen, Forschungsergebnisse (inkl. Dissertationen) des Instituts und des Archivs für deutsche Polarforschung, sowie Abstracts und Proceedings von nationalen und internationalen Tagungen und Workshops des AWI.

Die Beiträge geben nicht notwendigerweise die Auffassung des AWI wider.

Herausgeber
Dr. Horst Bornemann

Redaktionelle Bearbeitung und Layout
Birgit Reimann

Alfred-Wegener-Institut
Helmholtz-Zentrum für Polar- und Meeresforschung
Am Handelshafen 12
27570 Bremerhaven
Germany

www.awi.de
www.reports.awi.de

Der Erstautor bzw. herausgebende Autor eines Bandes der Berichte zur Polar- und Meeresforschung versichert, dass er über alle Rechte am Werk verfügt und überträgt sämtliche Rechte auch im Namen seiner Koautoren an das AWI. Ein einfaches Nutzungsrecht verbleibt, wenn nicht anders angegeben, beim Autor (bei den Autoren). Das AWI beansprucht die Publikation der eingereichten Manuskripte über sein Repositorium ePIC (electronic Publication Information Center, s. Innenseite am Rückdeckel) mit optionalem print-on-demand.

The Reports on Polar and Marine Research are issued by the Alfred Wegener Institute, Helmholtz Centre for Polar and Marine Research (AWI) in Bremerhaven, Germany, succeeding the former Reports on Polar Research. They are published at irregular intervals.

The Reports on Polar and Marine Research contain presentations and results of research activities in polar regions and in the seas either carried out by the AWI or with its support.

Publications comprise expedition reports of the ships, aircrafts, and stations operated by the AWI, research results (incl. dissertations) of the Institute and the Archiv für deutsche Polarforschung, as well as abstracts and proceedings of national and international conferences and workshops of the AWI.

The papers contained in the Reports do not necessarily reflect the opinion of the AWI.

Editor
Dr. Horst Bornemann

Editorial editing and layout
Birgit Reimann

Alfred-Wegener-Institut
Helmholtz-Zentrum für Polar- und Meeresforschung
Am Handelshafen 12
27570 Bremerhaven
Germany

www.awi.de
www.reports.awi.de

The first or editing author of an issue of Reports on Polar and Marine Research ensures that he possesses all rights of the opus, and transfers all rights to the AWI, including those associated with the co-authors. The non-exclusive right of use (einfaches Nutzungsrecht) remains with the author unless stated otherwise. The AWI reserves the right to publish the submitted articles in its repository ePIC (electronic Publication Information Center, see inside page of verso) with the option to "print-on-demand".

Titel: Waschtag auf Polarstern? Nicht wirklich. Die Leine mit den Stoffbändern ist das untere Ende des Kabels, an dem das neue Schleppsystem Triaxus/topAWI auf dem Transit von Punta Arenas nach Bremerhaven hinter dem fahrenden Schiff durchs Wasser gezogen wurde (Foto: Volker Strass, AWI).

Cover: Laundry day on Polarstern? Not really. The line with the garment ribbons is the lower end of the towing cable by which the new towed measuring system Triaxus/topAWI was pulled through the water behind the steaming ship during the transit from Punta Arenas to Bremerhaven (Photo: Volker Strass, AWI).

The Expedition PS113 of the Research Vessel POLARSTERN to the Atlantic Ocean in 2018

Edited by
Volker Strass
with contributions of the participants

Please cite or link this publication using the identifiers

http://hdl.handle.net/10013/epic.c161bfa4-7cfb-4c97-95e5-4ccadb3ce170 and
https://doi.org/10.2312/BzPM_0724_2018

ISSN 1866-3192

PS113

(Atlantic Transit)

Punta Arenas - Bremerhaven

08 May 2018 - 11 June 2018

Chief Scientist
Volker Strass

Coordinator
Rainer Knust

Contents

1. ÜBERBLICK UND FAHRTVERLAUF

Volker Strass AWI

Der Fahrtabschnitt PS113 deckte sich mit der Rückreise von *Polarstern* nach Beendigung der Antarktis-Forschungssaison 2017/18. Das für den Abend des 7. Mai geplante Auslaufen verzögerte sich auf Grund der etwas schwierigen Abläufe im Hafen von Punta Arenas, Chile, leider um einen Tag. Achterlicher Wind und ein starker, Richtung Atlantik setzender Gezeitenstrom in der Magellanstraße halfen uns aber, einen Teil der verloren gegangenen Schiffszeit gleich zu Beginn des Fahrtabschnitts wieder aufzuholen. Nach einem für Personalaustausch vorgesehenen Hafenanlauf in Las Palmas, Kanaren, am 03. Juni endete PS113 planmäßig am 11. Juni frühmorgens in Bremerhaven.

Da der größte Teil (ca. 9/10) der zur Verfügung stehenden Schiffszeit allein für das Zurücklegen der Fahrtstrecke Punta Arenas – Bremerhaven bei ökonomischer Marschfahrt von *Polarstern* benötigt wurde, war die Zeit für wissenschaftliche Stationsarbeiten sehr begrenzt. Der Schwerpunkt lag deswegen auf Forschungsarbeiten, die vom fahrenden Schiff aus entlang des Transit-Kurses durchgeführt werden konnten. Dazu gehörte auch das Haupt-Vorhaben während PS113, die Indienststellung des neuen geschleppten Messsystems Triaxus/topAWI (towed ocean profiler of the AWI) auf *Polarstern*.

Die Indienststellung von Triaxus/topAWI umfasste vielfältige Arbeiten an Bord: Die Positionierung der Schleppwinde, die Optimierung der Schleppdrahtführung über Deck, das Aufstellen der Rechner für die Systemsteuerung und Datenerfassung, die Einbindung ins Bord-Datennetz, Funktionstests sowie Kalibrierungen von Messinstrumenten und Sensoren, die Überprüfung des Schleppkörper-Verhaltens während verschiedener Schlepp-Modi, die Ermittlung optimaler Steuerparameter (Auf- und Abtauchgeschwindigkeiten, Vertikalamplituden, seitliche Auslenkungen usw.) für unterschiedliche Schiffsgeschwindigkeiten und Drahtlängen, das Einüben der Aussetz- und Einholprozeduren, das Erstellen der entsprechenden Protokolle, die Schulung von Personal aus verschiedenen Fachbereichen und auch die Identifikation von Problemen. Die dabei gemachten Erfahrungen haben bestätigt, dass die während PS113 dafür genutzte Schiffszeit zwingend notwendig war, um das neue Schleppsystem auf nachfolgenden Forschungsreisen operationell einzusetzen zu können. Die während der Indienststellung nebenbei gesammelten Messdaten zeigen das hervorragende wissenschaftliche Potential von Triaxus/topAWI, viele physikalische, chemische und biologische Variable simultan und quasi-synoptisch mit hoher zeitlicher und räumlicher Auflösung sowie Überdeckung zu messen. So können jene Prozesse genauer identifiziert werden, welche die Phytoplankton-Photosynthese sowie Primärproduktion und damit auch die CO_2-Aufnahme und letztendlich Fischerei-Erträge beeinflussen.

Die Indienststellung von topAWI wurde begleitet von Vergleichsmessungen mit etablierten Messverfahren wie hydrographischen Stationen und Vertikalprofilen von optischen Parametern des Ozeanwassers. Letztere zielen zudem darauf ab, Satelliten-Sensoren der Ozean-Farbe zu validieren und damit die Fernerkundung von Phytoplankton-Konzentrationen zu verbessern. Regelmäßig für genetische Untersuchungen genommene Wasserproben werden es ermöglichen, meridionale Unterschiede der Plankton-Artenzusammensetzung beim Durchqueren verschiedener Klimazonen während des Transits zu identifizieren. Oberflächen-

Wellen und -Strömungen wurden mittels des WaMoS-Radarsystems aufgezeichnet und ausgewertet. Als Beitrag zum internationalen globalen Ozean-Beobachtungsprogramm Argo wurden drei autonome, Temperatur- und Salzgehalt profilierende Treibkörper im Süd-Atlantik ausgebracht, der hinsichtlich der Datenlage bislang unterrepräsentiert ist.

Änderungen von Atmosphären-Eigenschaften und -Prozessen zwischen der Südhemisphäre und der von menschlichen Aktivitäten stärker gestörten Nordhemisphäre wurden durch den Einsatz eines hochentwickelten Lidar-Systems sowie von Sonnen-Photometern erfasst. Am Meeresboden wurden bathymetrische Kartierungen und Sediment-Profilierungen mittels verschiedener auf *Polarstern* installierter Sonar-Systeme durchgeführt. Nicht zuletzt wurden Fische, die zuvor in antarktischen Gewässern gefangen wurden, lebend in Aquarien gehältert, versorgt und ans AWI für weitere physiologische Untersuchungen verbracht.

SUMMARY AND ITINERARY

The cruise leg PS113 coincided with the return voyage of *Polarstern* after finishing her Antarctic research season 2017/18. PS113 started on the evening of 08 May, delayed by one day due to the somewhat difficult arrangements at the harbour of Punta Arenas, Chile. Tailwinds and a strong tidal current setting towards the Atlantic in the Strait of Magellan, but helped us to regain part of the lost ship time right at the beginning of the cruise. As planned, an intermediate port call at Las Palmas, Canary Islands, took place on 03 June for the exchange of personnel. According to schedule PS113 ended in Bremerhaven early on 11 June 2018.

Most of the time (ca. 9/10) allocated to PS113 was used simply for transiting between Punta Arenas and Bremerhaven at an economically reasonable steaming speed. The ship time available for scientific station work hence was very limited. Emphasis thus was laid on research work that could be conducted *en route* along the transit course. This encompasses the main scientific project during PS113, the commissioning of a new measuring system, the Triaxus towed ocean profiler of the AWI (topAWI).

The commissioning of Triaxus/topAWI encompassed a variety of tasks: the positioning of the tow-winch on the working deck, optimization of the cable routing, placement of computers for system control and data acquisition, connection to the ships data network, function control and calibrations of scientific instruments and sensors, examination of the vehicle performance during various towing modi, determination of optimal towing parameters (dive and climb velocities, vertical amplitudes, horizontal offsets etc.) at different ship speeds and towing cable lengths, practice of deployment and recovery procedures, development of the pertinent protocols, training of personnel from different disciplinary departments, and also the identification of problems. Experiences gathered during the commissioning confirmed that the shiptime of PS113 assigned for it was an indispensable prerequisite for operational deployments of the new system during future research cruises. First data collected *en route* demonstrated the excellent scientific potential of Triaxus/topAWI to measure simultaneously - with high temporal and spatial coverage and resolution in a quasi-synoptic manner - many physical, chemical and biological variables that are relevant to identify the processes which control phytoplankton photosynthesis and primary production, hence the uptake of CO_2 and the formation of the basis of the marine food webs and ecosystems.

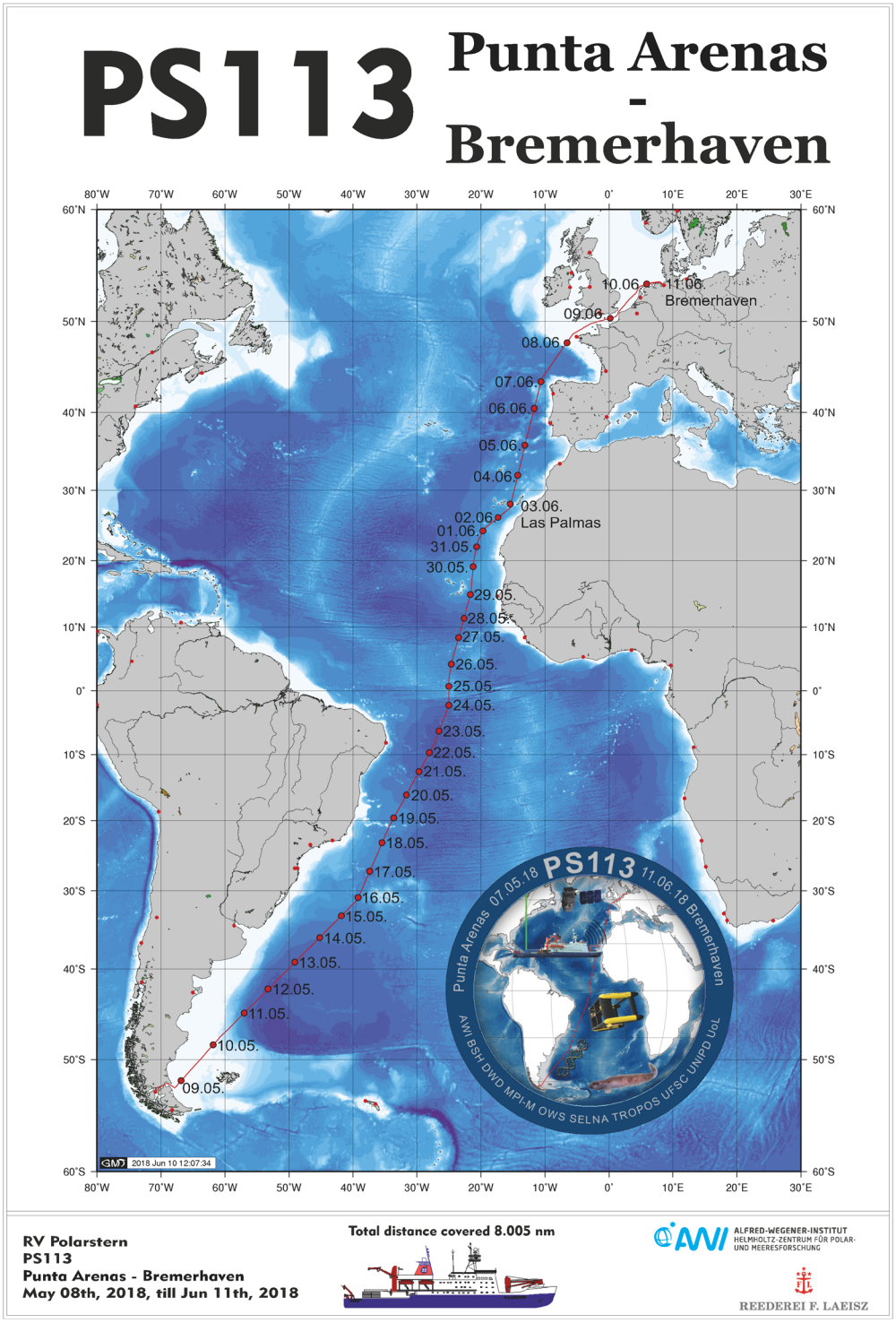

Abb. 1: Fahrtroute der Polarstern Expedition PS113 von Punta Arenas nach Bremerhaven mit täglichen Zeitmarken (rote Punkte). Siehe https://doi.pangaea.de/10.1594/PANGAEA.891753 für eine Darstellung des master tracks in Verbindung mit der Stationsliste für PS113.

Fig. 1.1: Cruise track of RV Polarstern during expedition PS113 from Punta Arenas to Bremerhaven with daily time stamps (red dots). See https://doi.pangaea.de/10.1594/PANGAEA.891753 to display the master track in conjunction with the list of stations for PS113.

For inter-calibration purposes, the commissioning of Triaxus/topAWI was accompanied by measurements carried out with proven techniques, such as hydrographic stations enhanced by vertical profiling of ocean optical properties. The latter is also aimed at the validation of ocean colour satellite sensors hence at improved remote sensing of phytoplankton concentrations. Samples taken regularly for plankton genomics will allow for an assessment of the meridional differences in plankton species diversity, which go along with the different climatic zones crossed during the transit. Surface waves and currents were determined by the radar-based WaMoS system of *Polarstern*. As a contribution to the international global ocean observing programme Argo, three autonomous temperature/salinity profiling floats were deployed in the South Atlantic Ocean that has not yet been sufficiently sampled.

Changes in atmospheric properties and processes underway from the Southern Hemisphere, which is less perturbed by human activities, and the more disturbed Northern Hemisphere were revealed using advanced lidar systems and sun-photometers. Deepest down at the seafloor and in the sediments, bathymetric mapping and sub-bottom profiling was conducted using various sonar systems installed on *Polarstern*. Last but not least, fish caught before in Antarctic waters were held live in aquaria, were attended to and transported to AWI for extended physiological investigations.

2. WEATHER CONDITIONS

Max Miller[1], Juliane Hempelt[1] [1]DWD

On Tuesday evening, May 08, 2018, 18:20 pm, *Polarstern* left Punta Arenas for the campaign PS113. Light north-westerly winds, 13° C and mostly cloudy skies were observed.

Over Drake Passage and Tierra del Fuego strong westerly winds were still prevailing. Right after leaving the harbour winds freshened up to 6 to 7 Bft. Steaming the Strait of Magellan winds were influenced by orography, too. Entering the South Atlantic on Wednesday morning (May 09) winds abated at a sea state of less than 2 m.

During the night to Friday (May 11) a low formed over the mouth of the La Plata River. It deepened to a storm and moved quickly southeast. Furthermore a secondary low developed north of the Falkland Islands, which moved northeast. *Polarstern* got at the west side of that system. Winds veered southwest (tail wind) and increased steadily, peaked for short times at 10 Bft on late Saturday afternoon and forced a sea state up to 6 m. During the night to Sunday (May 13) the southerly winds started to abate already, on Sunday evening we observed only 3 Bft.

On Monday (May 14) *Polarstern* reached the southern end of a high off Brazil. The high moved east and during the night to Tuesday we got at its west side. Winds veered north and increased up to 6 to 7 Bft. At the same time a low south of Bahia Blanca headed towards South Georgia. Its cold front with embedded thunderstorms caught up with *Polarstern* on Wednesday morning (May 16) – still at 7 Bft. Afterwards winds veered southwest and abated.

On Friday (May 18) *Polarstern* got at the northwest side of a high over South Atlantic at north-easterly winds around 5 Bft. From Whit Monday (May 21) on we steamed the southern trade winds, which peaked at 6 Bft. Isolated showers were still present.

On Thursday evening (May 24) *Polarstern* entered the inner tropical convergence zone (ITCZ) located close to the equator. Winds abated clearly but showers became more and stronger. But we did not observe any thunderstorm.

From the night to Sunday (May 27) on *Polarstern* sailed the northern trade winds, which blew mostly at 5 to 6 Bft. Only along the east coast (parallel to the wind) of Gran Canary northerly winds peaked at 8 Bft for short times. Especially during the first part of the trade wind zone Sahara Dust enriched the atmosphere.

On Sunday morning (June 03) we reached Las Palmas and left the harbour in the afternoon at northerly winds 4 to 5 Bft.

First we steamed at the northeast side of the high near the Azores. Winds up to 5 Bft veered gradually west. On Wednesday (June 06) a secondary low built at the southeast side of a low south of Greenland and headed towards Cape Finisterre. Its cold front crossed *Polarstern* on Thursday morning. North-westerly winds freshened up to 6 Bft, but abated during the course of the day.

A weak low over Central and Western Europe with several small centres was the dominant feature during the remaining journey. Light to moderate winds veered east to northeast and

increased temporarily up to 6 Bft while passing the English Channel on Saturday (June 09). Fog patches were present there, too. Over the Southern North Sea winds veered finally northwest.

On late Sunday evening, June 10, 2018, *Polarstern* reached Bremerhaven at temporarily freshening north-westerly winds.

For further statistics see attached files (Fig. 2.1 – Fig. 2.3).

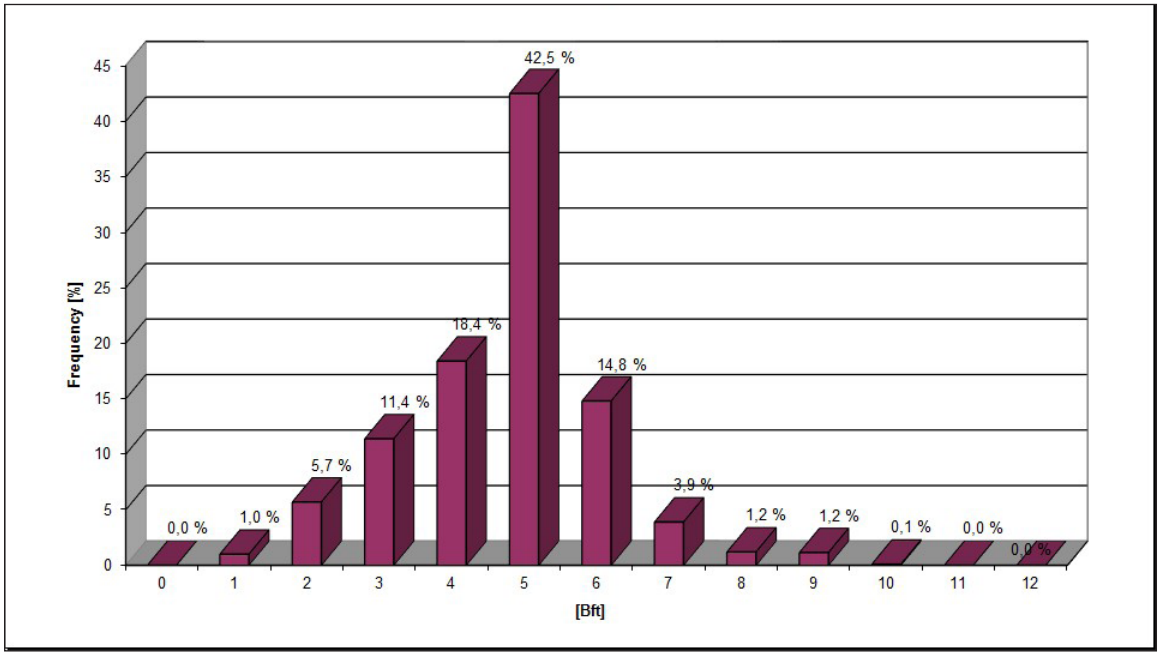

Fig 2.1: Distribution of wind force during PS113

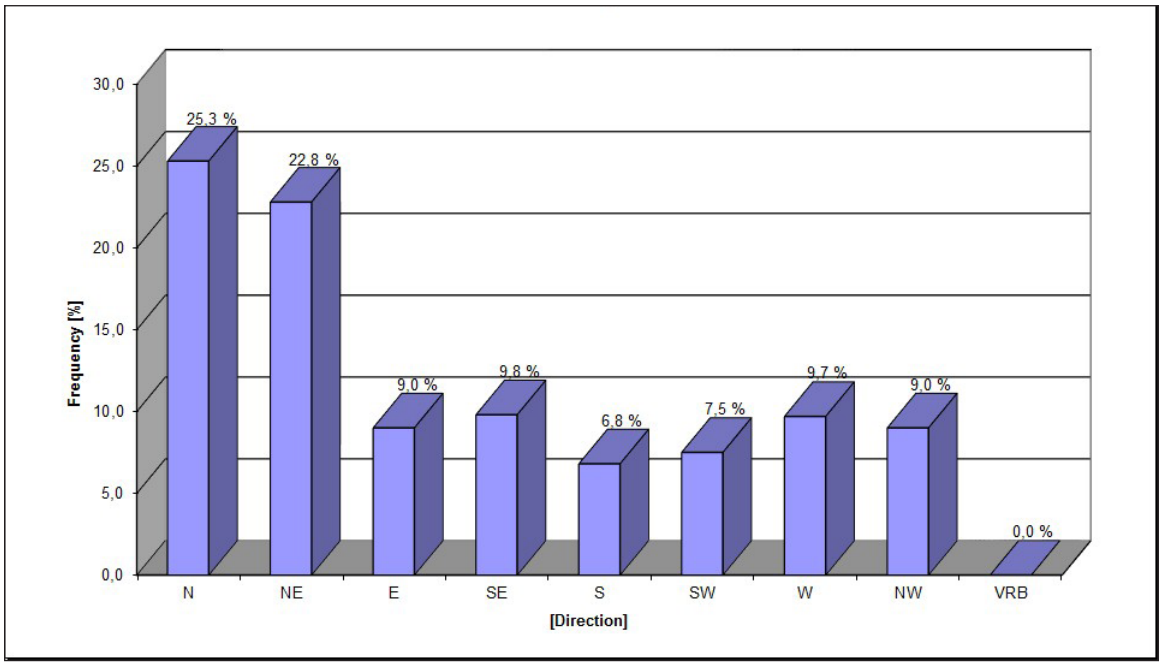

Fig 2.2: Distribution of wind direction during PS113

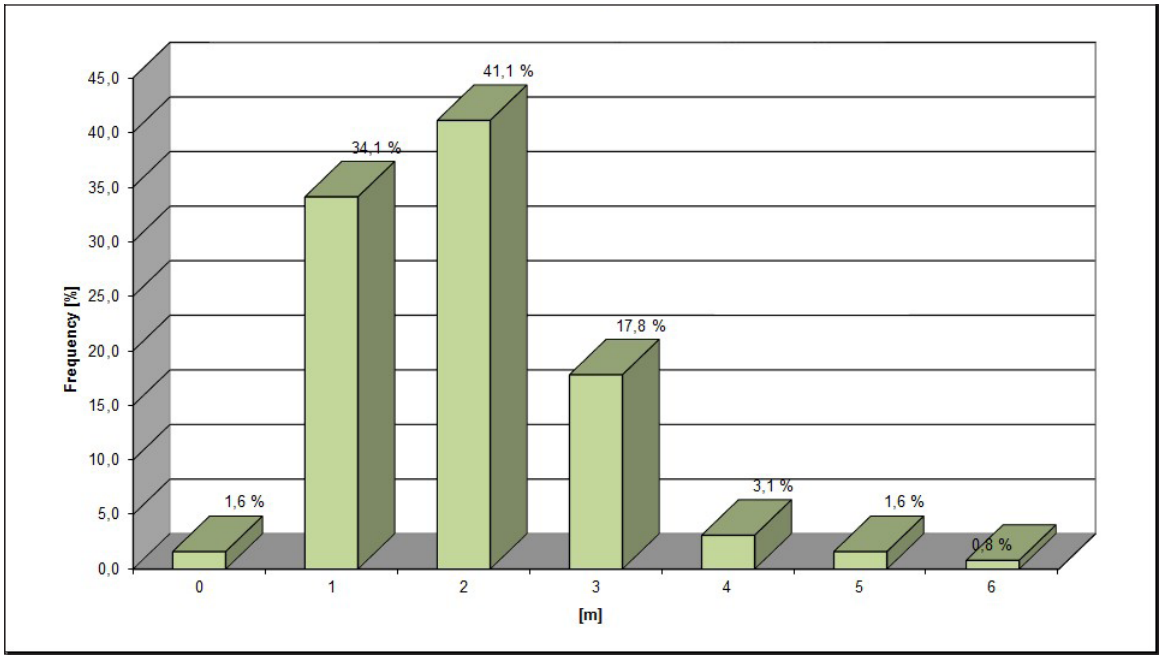

Fig 2.3: Distribution of sea state during PS113

3. SYSTEM-TESTING AND COMMISSIONING OF THE MULTIDISCIPLINARY TOWED OCEAN PROFILER OF THE AWI (TOPAWI)

Volker Strass[1], Astrid Bracher[1], Hauke Flores[1] (not on board), Saad El Naggar[2], Hauke Haake[1], Jonas Hagemann[1] (disembarked Las Palmas), Harry Leach[3], Susanne Spahić[1], Augusto Neubauer[4], Sven Lenius[1], Wilken-Jon von Appen[1], Anya Waite[1] (embarked Las Palmas)

[1]AWI
[2]RFL
[2]UoL
[4]UFSC

Grant-No. AWI_PS113_00

Objectives

The oceans play a key role within the Earth system, inter alia by the sequestration and global-scale redistribution of heat, CO_2, and nutrients. They harbor diverse marine ecosystems, which yield living resources and effect biogeochemical fluxes that influence global climate. The ecosystems change with the physical and chemical environments, in ways which are however not completely identified. To better understand the functioning of marine systems with their high degree of complexity resulting from the interaction of physical, chemical and biological processes, measurements are needed that comprise the different disciplines and that are taken simultaneously over a very wide range of temporal and spatial scales and trophic levels.

Measuring simultaneously the relevant physical, chemical and biological variables with high temporal and spatial coverage and resolution in a quasi-synoptic manner represents a challenge that can best be met by towed undulating vehicles that have sufficient payload capacity. To this end, AWI recently purchased a vehicle-winch system type Triaxus E from MacArtney, Denmark, modified and instrumented to AWI's scientific needs and termed topAWI, the towed ocean profiler of AWI. It is designed to achieve a vertical undulation range of 450 m below surface, once the optimal combination of towing speed and tow cable length have been assessed, and provided the scientific payload is pressure resistant down to that depth and hydrodynamically not too obstructive. The large vertical undulation is achieved by an automatic winch control embedded in the vehicle steering software, which directs the winch to pay out and retrieve cable on demand. The vehicle is also able to sheer out to the side of the ship track, in order to obtain vertical profiles close to the surface outside the propeller wash in water undisturbed by the ship. At present, the basic scientific payload comprises a CTD sonde for determination of temperature, salinity, depth (and density), oxygen sensor, fluorometer for chlorophyll concentration, light transmissiometer, PAR sensor for photosynthetically available radiation, hyperspectral radiometer, pair of up- and downward looking acoustic Doppler current profilers (ADCPs), and a broad-band acoustic zooplankton sounder. Other auxiliary sensors such as altimeters (up- and down-looking), acoustic transponder and radio beacon serve the vehicles surveillance and safety. Figures 3.1 – 3.4 show photographs taken during launch operations of the Triaxus vehicle, and its instrumentation from different perspectives.

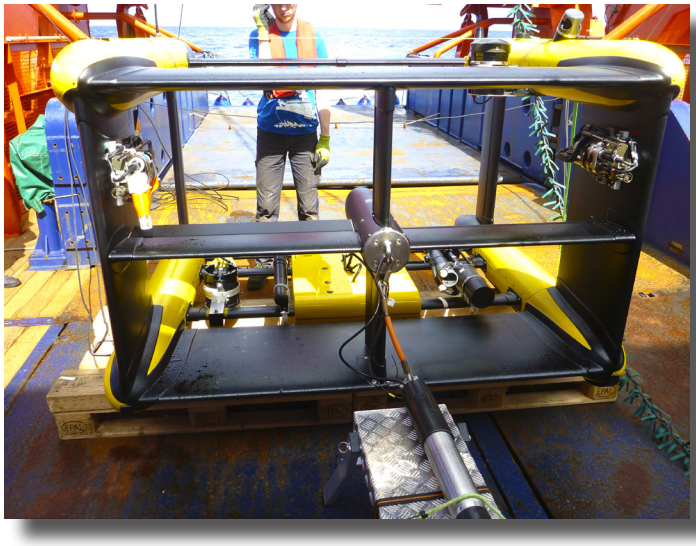

Fig. 3.1: Front view of the vehicle during a pre-dive check (Foto: V. Strass)

Fig. 3.2: Bottom view of vehicle during its lift for deployment (Foto: H. Leach)

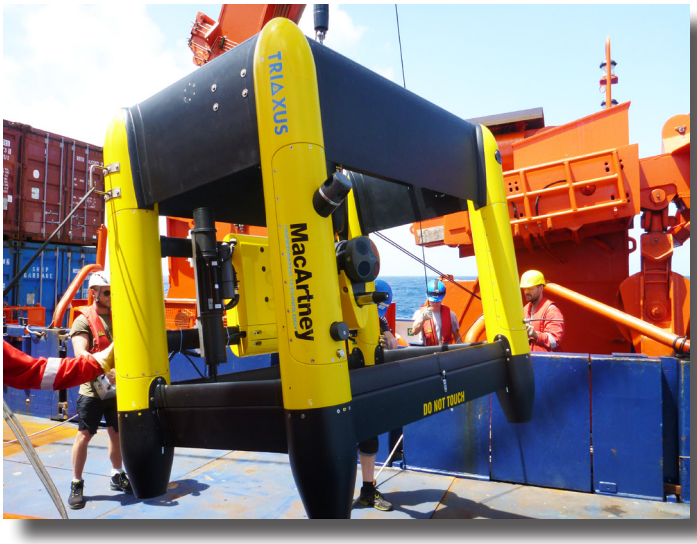

Fig. 3.3: Top view of the vehicle while moved towards the stern for deployment (Foto: V. Strass)

Work at sea

A complex, new and unique system such as topAWI needs intensive testing at sea after completion and initial instrument integration. This system testing was the major project during PS113, which likewise constituted the commissioning cruise of topAWI on *Polarstern*.

Fig. 3.4: Triaxus being launched (Foto: V. Strass)

Work on topAWI started already in the port of Punta Arenas with the placement of the containerized winch holding the towing cable (Fig. 3.5), the guiding of the towing cable across the aft deck (Fig. 3.6) that encompassed the mounting of one special block on the A-frame and another one between working deck and helicopter deck directly behind the winch container. Also done already in port was the buoyancy check of the Triaxus vehicle including the complete scientific payload. After leaving Punta Arenas, deck unit, PCs for system control and data acquisition, were rigged up one deck above the working deck next to the winch control room (Fig. 3.7) and all components were connected with each other and with the ship's data network. Fig. 3.8 depicts schematically the distribution of the major system components on *Polarstern*.

Fig. 3.5: Winch with towing cable in its container housing (Foto: V. Strass)

Fig. 3.6: Towing cable path and guiding over the aft deck; the turning block next to the winch container is seen in the bottom right corner (Foto: V. Strass)

Deployments for sea trials (summarized in Table 3.1) started on May 11, once the exclusive economic zones of Argentina and the United Kingdom were passed and left. Deployments served various purposes as there were:

- Check the functioning of the complete system including all components
- Assess its operability on board *Polarstern*
- Determine and optimize the flight performance of the vehicle in dependence of varying tow parameters such as ship speeds, cable lengths, vertical undulation ranges, dive and rise rates, and horizontal offset angles

- Identify contingent technical problems, shortcomings and possible improvements
- Appraise the scientific potential of the new system at its present payload configuration
- Improve the procedures of launch and recovery, and document them in protocols
- Train personnel from various disciplines and science departments in the use of Triaxus/ topAWI for future research cruises

Fig. 3.7: Triaxus control centre with deck unit (blue box) and various laptops for running the steering software and programmes for data acquisition, rigged up in the Scientific Working Room II of Polarstern, which deigns a look to the aft deck where the winch is placed (Foto: V. Strass).

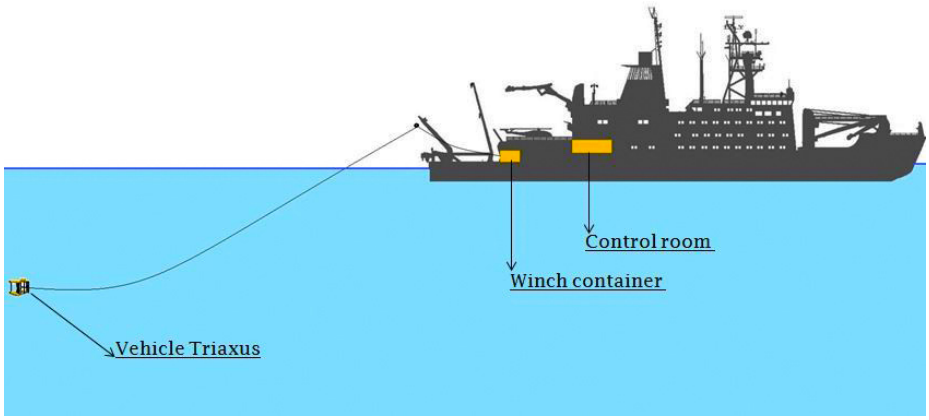

Fig. 3.8: Placement of main components of the topAWI system on board Polarstern

Tab. 3.1: Deployments of the Triaxus/topAWI vehicle

Depl.-No	Stn.-File	Start			End			Activity
		Date time [UTC] dd.mm.yyyy HH:MM	Latitude	Longitude	Date time [UTC] dd.mm.yyyy HH:MM	Latitude	Longitude	
1	PS113_002-01	11.05.2018 11:59	-45.0988	-57.0097	11.05.2018 14:09	-44.9122	-56.7468	Initial system and sensor check
2	PS113_004-01	11.05.2018 17:56	-44.8163	-56.5963	11.05.2018 21:38	-44.5089	-56.1600	System function verification
3	PS113_008-01	14.05.2018 17:20	-35.6447	-44.6284	14.05.2018 21:06	-35.3117	-44.2203	Winch inspection and test
4	PS113_012-01	16.05.2018 16:08	-30.5546	-38.9763	16.05.2018 19:19	-30.2113	-38.8252	Winch adjustment
5	PS113_016-01	19.05.2018 13:33	-19.4711	-33.5428	19.05.2019 18:05	-19.0122	-33.2794	CTD test
6	PS113_019-01	21.05.2018 14:04	-12.5131	-29.6286	21.05.2018 18:00	-12.2904	-29.5094	ADCP calibration
7	PS113_020-02	22.05.2018 10:20	-9.7670	-28.1126	22.05.2018 18:14	-9.1800	-27.8013	GAPS horizontal offset test
8	PS113_024-01	24.05.2018 13:47	-2.2240	-25.0332	25.05.2018 22:41	2.1303	-24.9806	Payload assessment across equator
9	PS113_027-03	27.05.2018 11:42	8.3030	-23.5238	27.05.2018 18:19	9.0969	-23.2949	Undulation auto spool and EK80 test
10	PS113_028-03	28.05.2018 10:41	11.2012	-22.7009	28.05.2018 17:39	12.2103	-22.4030	9/10 knots flight performance test
11	PS113_029-03	30.05.2018 17:33	19.8071	-21.1470	31.05.2018 16:00	22.5669	-20.5310	Payload assessment in upwelling region
12	PS113_031-03	01.06.2018 10:07	24.1878	-19.8187	01.06.2018 16:51	24.7297	-19.4331	GAPS horizontal undulation test
13	PS113_032-01	05.06.2018 05:30	35.3560	-13.2957	05.06.2018 10:19	35.9544	-13.1151	Control software test

For comparison of the measurements made with the new instruments installed on Triaxus/topAWI, data were also collected using established methods and gear, such as hydrographic stations with vertical casts of the CTD (SBE 911plus) integrated with a Carousel Water Sampler, and with an optical instruments package. Both CTD and optics package casts were conducted at approximately regular daily intervals until port call in Las Palmas on June 3. Tab. 3.2 lists the CTD stations; the casts with optical instruments package are presented later in Chapter

4. Most of the CTD casts were limited to the upper 400 m of the water column, just sufficient to encompass the depth range of the Triaxus vehicle, which in its present configuration is restricted to 350 m by the pressure rating of some of the installed optical instruments and of the buoyancy foam elements. Fig. 3.9 illustrates the hydrographic and biogeochemical background information (potential temperature, salinity, concentration and deficit of dissolved oxygen, chlorophyll fluorescence, and light attenuation) as obtained by the CTD from Stations 1 through 31.

Tab. 3.2: Hydrographic stations with casts of the CTD and Carousel Water Bottle Sampler

Station	Date Time (Max Depth)	Latitude	Longitude	Water Depth [m]	Max. Instr. Depth [m]
PS113_1-2	10.05.2018 18:26	47° 38.876‘ S	060° 42.786‘ W	393	383
PS113_3-2	11.05.2018 15:34	44° 53.834‘ S	056° 45.669‘ W	4999	401
PS113_5-2	12.05.2018 15:25	42° 09.322‘ S	052° 51.793‘ W	5626	398
PS113_6-2	13.05.2018 15:27	38° 52.630‘ S	048° 38.987‘ W	5293	399
PS113_7-2	14.05.2018 15:54	35° 47.335‘ S	044° 46.756‘ W	4865	399
PS113_9-2	15.05.2018 14:53	33° 07.038‘ S	041° 35.558‘ W	4572	399
PS113_10-1	16.05.2018 07:56	31° 12.486‘ S	039° 18.942‘ W	4543	4475
PS113_11-2	16.05.2018 14:53	30° 41.206‘ S	039° 02.260‘ W	4137	401
PS113_13-2	17.05.2018 14:29	27° 03.746‘ S	037° 15.894‘ W	4583	401
PS113_14-2	18.05.2018 14:54	22° 59.552‘ S	035° 20.352‘ W	4213	401
PS113_15-1	19.05.2018 11:29	19° 35.871‘ S	033° 36.913‘ W	4163	402
PS113_17-2	20.05.2018 14:49	15° 56.464‘ S	031° 33.411‘ W	4737	401
PS113_18-2	21.05.2018 13:36	12° 31.551‘ S	029° 38.196‘ W	5531	402
PS113_20-1	22.05.2018 09:26	09° 46.535‘ S	028° 07.402‘ W	5657	1001
PS113_21-1	22.05.2018 18:22	09° 10.672‘ S	027° 48.033‘ W	5686	1000
PS113_22-2	23.05.2018 12:59	06° 16.690‘ S	026° 35.461‘ W	5683	402
PS113_23-2	24.05.2018 13:24	02° 13.790‘ S	025° 01.979‘ W	4611	402
PS113_25-1	25.05.2018 23:15	02° 08.341‘ N	024° 58.967‘ W	not measured	409
PS113_26-2	26.05.2018 12:13	04° 10.111‘ N	024° 38.094‘ W	4613	399
PS113_27-1	27.05.2018 10:16	08° 17.777‘ N	023° 31.502‘ W	4898	400
PS113_28-1	28.05.2018 09:15	11° 11.474‘ N	022° 41.641‘ W	5106	401
PS113_29-2	30.05.2018 17:07	19° 48.240‘ N	021° 09.150‘ W	3664	402
PS113_30-2	31.05.2018 17:52	22° 36.739‘ N	020° 32.759‘ W	4221	400
PS113_31-1	01.06.2018 08:19	24° 09.348‘ N	019° 48.315‘ W	3657	554
PS113_33-1	05.06.2018 10:40	35° 57.381‘ N	013° 07.128‘ W	4845	201

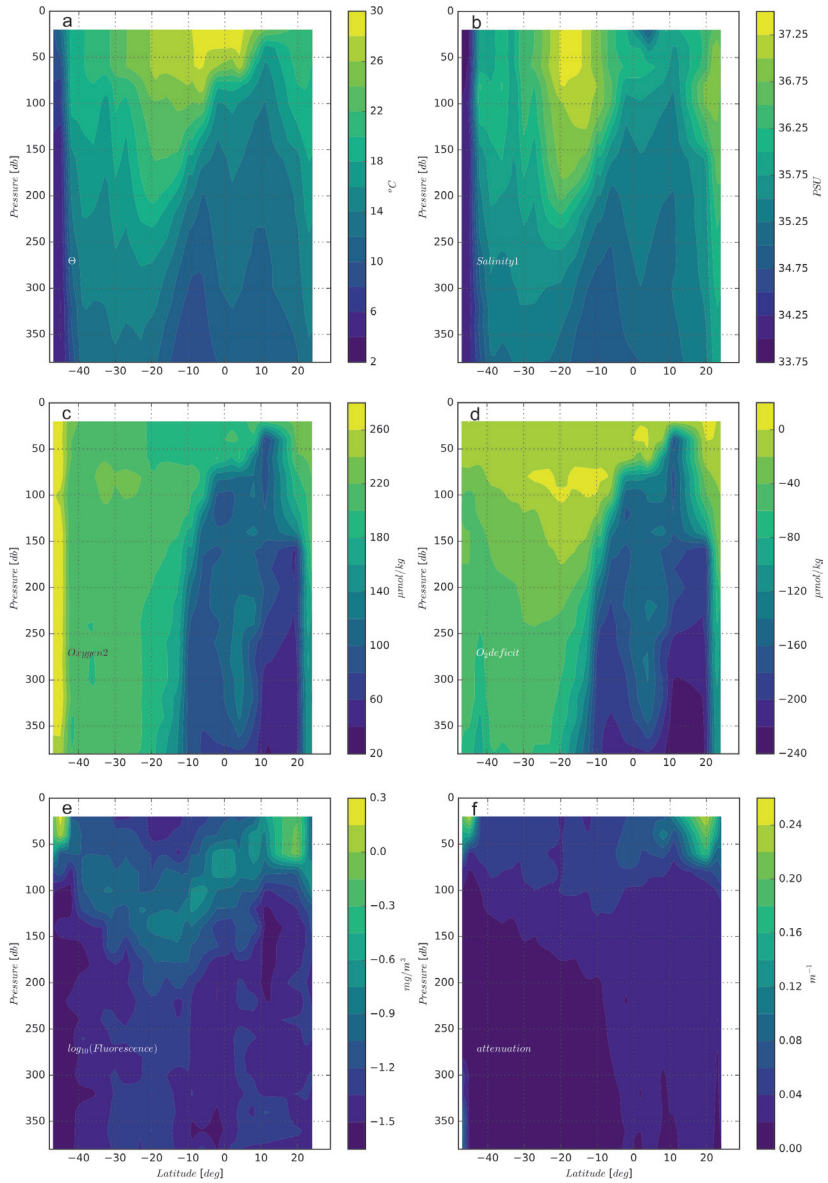

Fig. 3.9: Transatlantic section of potential temperature (a), salinity (b), concentration of dissolved oxygen (c), deficit of dissolved oxygen (d), logarithm of chlorophyll fluorescence (e), and light attenuation at 650 nm (f) derived from CTD casts made at an average latitudinal distance of 2.3° or 257 km, respectively.

Further cross-validations were conducted with data collected underway, such as by the thermosalinograph and by the vessel-mounted acoustic Doppler current profiler (VM-ADCP) of *Polarstern* (type 'Ocean Surveyor', manufacture of RDI, with 150 kHz nominal frequency). The VM-ADCP data recording was split in the 4 segments listed in Table 3.3; the data gap between 29 May and 4 June results from the fact that we had switched off the ADCP when passing through the Spanish EEZ around the Canary Islands as a precautionary measure in order of not disturbing a regional beaked whale population, following an recommendation of the Spanish Ministry of Foreign Affairs and Cooperation.

Tab. 3.3: Underway current profile data recorded with the VM-ADCP

Record	Begin [date time UTC]	End [date time UTC]
PS113001	10.05.2018 16:55	27.05.2018 21:52
PS113002	27.05.2018 22:01	29.05.2018 02:02
PS113003	29.05.2018 08:22	01.06.2018 17:19
PS113004	04.06.2018 07:27	07.06.2018 17:12

Preliminary results

The tests of Triaxus/topAWI conducted during PS113 yielded the experiences that are stringently required as a solid basis for successful deployments during future research cruises.

- Participants from three different scientific disciplines/research departments have gained a deeper insight into the hard- and software components and their coaction.
- Launch and recovery procedures were much improved and speeded up, and documented in protocols.
- An optimized set of recommended vehicle control parameters was determined for the present payload configuration. For example, a regular vertical undulation between 5 and 350 m can be achieved at 8 knots ship speed with a cable length of 1,800 – 1,900 m, applying descent and ascent velocities of 1 m s-1. With these settings an up and down cycle is completed within less than 12 min., resulting in a horizontal resolution (wavelength) of 2.9 km.
- Identified technical problems have either been reported to the manufacturer with the request for solution (restricted functionality of the auto-depth mode of the steering software, spooling irregularities of the winch) or will be fixed at the AWI (changeability of up/down-looking orientation of the acoustic zooplankton sounder).
- Longer continuous tows in regions of expected strong gradients (for 33 hours across the equator and for 22 hours through the Northwest African upwelling regime) resulted in measurements which demonstrate the scientific potential of the new system for interdisciplinary research into the physical controls of primary production and the phytoplankton-related underwater light filed and of biogeochemical fluxes.

Fig. 3.10 illustrates how much detail in the distribution of environmental variables is revealed by the high horizontal resolution achieved with Triaxus/topAWI. This example was taken from the tow across the equator with its Equatorial Undercurrent, a feature that strongly effects the environmental variability, which was not resolved by the coarse spacing of CTD casts made during the cruise (see Fig. 3.9 for comparison).

Data management

The metadata of the scientific measurements made during PS113 have been transmitted two months after the cruise in form of the Cruise Summary Report (CSR) to the Deutsches Ozeanographisches Datenzentrum (DOD). All data will be deposited step by step after processing in the PANGAEA Data Publisher for Earth & Environmental Science, a database accessible to the public. We expect all data to become publically available within two years after completion of the cruise.

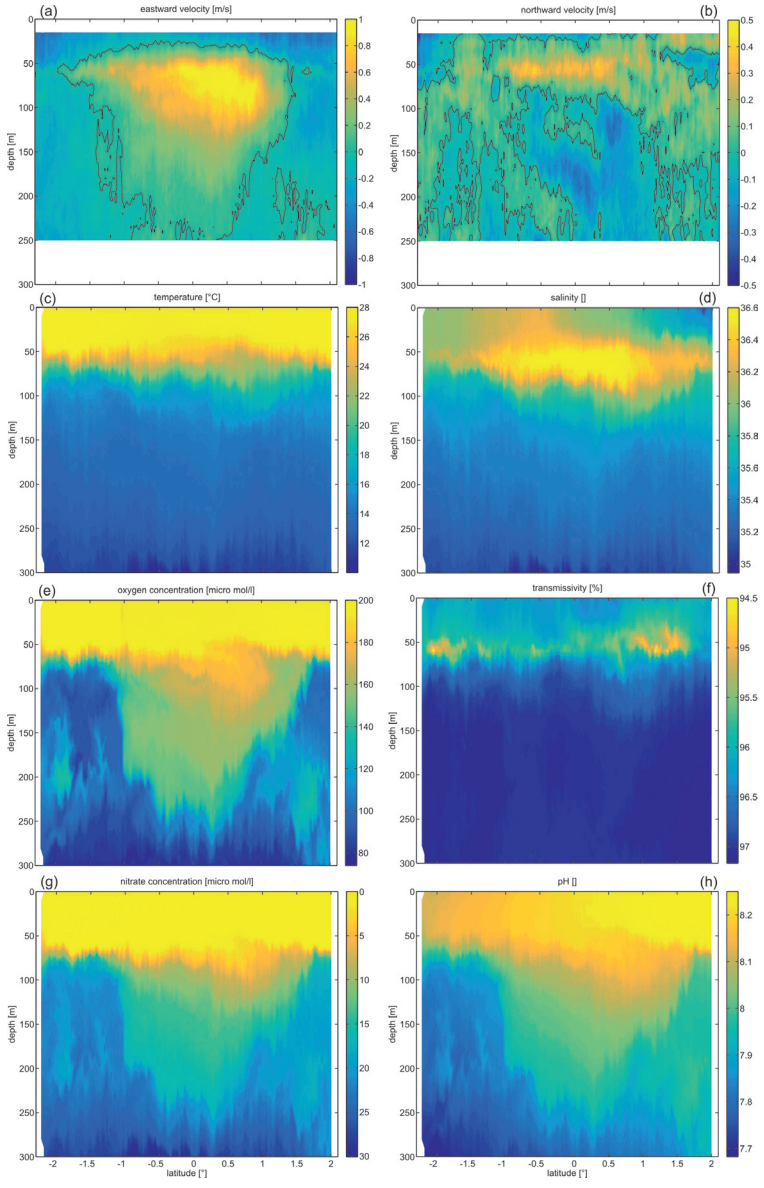

Fig. 3.10: Equator cross-section of the eastward and northward velocity components measured by the vessel-mounted ADCP (a, b) and of potential temperature (c), salinity (d), concentration of dissolved oxygen (e), light transmissivity at 650 nm (f), nitrate concentration (g) and acidity value pH (h), measured by instruments mounted on Triaxus/topAWI. At the 300 m vertical undulation depth range set for the equator crossing the Triaxus/topAWI data have a horizontal resolution (wavelength) of 2.5 km, i.e. the section shown is composed of nearly 200 downward oriented vertical profiles. Please note the reversed colour scales used in panels f and g, chosen to ease visual identification of anti-correlations, in case of f with particulate organic carbon (POC, not shown).

4. OPTICAL PROPERTIES USED TO DERIVE CONTINUOUS DATA SETS ON PHYTOPLANKTON, PARTICULATE AND DISSOLVED ORGANIC MATTER

Astrid Bracher[1,2], Sonja Wiegmann[1], Hongyan Xi[1]

[1]AWI
[2]IUP

Grant-No. AWI_PS113_00

Objectives

Marine phytoplankton is the basis of the marine food web and also a main component of biogeochemical fluxes, thus, an important source of dissolved and particulate organic substances, including volatile organic substances (e.g. DMS, isoprene, halocarbons). During *Polarstern* cruise PS113 we focused to broaden our sampling frequency of information on phytoplankton, particulate and chromophoric dissolved organic matter (CDOM) abundance and composition by taking continuous optical measurements which directly give information on inherent and apparent optical properties (IOPs, and AOPs, respectively). These can later be inverted to extract information on the above listed parameters. The specific objectives of our group were to

- collect a high spatial and temporal resolved data set on phytoplankton (total and composition) and its degradation products at the surface and for the full euphotic zone using continuous optical observations during the cruise and from ocean colour remote sensing calibrated with discrete water sample measurements,
- develop and validate (global and regional) algorithms and associated radiative transfer models in accordance to the previous objective by using discrete water samples for pigment analysis and absorption measurements,
- obtain a big data set for ground-truthing ocean color satellite data, specifically from the new Sentinel-3 (A and B) OLCI and the Sentinel-5-Precursor TROPOMI sensors,
- assess the quality of optical data collected by the new Triaxus/topAWI system via instrument calibration, monitoring and comparison with to the optical measurements made underway and at stations,
- identify bio-physical-chemical coupling through cooperation with partners among the PS113 scientific party by using these comprehensive data sets to detect shifts in phytoplankton community, biomass and composition, and the factors driving the variability and changes in phytoplankton community and its degradation products.

Work at sea

In the following we state the methods we used to obtain quantity and composition of phytoplankton, other particulates and chromophoric dissolved organic matter (CDOM) from optical measurements.

a) Continuous and discrete measurements of inherent optical properties (IOPs) with hyperspectral spectrophotometers: For the continuous underway surface sampling an in-situ–spectrophotometer (AC-S; Wetlabs) was operated in flow-through mode to obtain total and particulate matter attenuation and

absorption of surface water with high spectral (~3.3 nm) resolution from 400 to 800 nm. The instrument was mounted to a seawater supply taking water from about 11 m depth through the teflon tubing with a membrane pump. A second AC-S instrument was mounted on a steel frame together with a depth sensor (and a set of radiometers - see point d) and operated after or before CTD stations. The frame was lowered down to maximally 130 m with a continuous speed of 0.1 m/s or with additionally stops to the maximum depth which depended on the incoming solar radiation to allow a better collection of radiometric data (see later). A third AC-s instrument was mounted on the Triaxus/topAWI vehicle and operated during all deployments. The second and third AC-s instrument only obtained total absorption and attenuation data, since no filter could be mounted to the instruments during operation in water. All three instruments were regularly calibrated by taking measurements of MilliQ water. The flow-through AC-s was calibrated daily, the discrete station profiling AC-s was calibrated after every 2 casts and the Triaxus-AC-s was calibrated before each Triaxus deployment.

b) Discrete measurements of IOPs (absorption) at water samples were performed 1) for samples from the underway surface sampling (as for the AC-s flow-through system at 11 m depth sampled from the ship's sea water supply via the membrane pump through the Teflon tubing) at an interval of 3 hours, and 2) for samples from the CTD rosette at 6 depths within the surface ocean (mostly top 100 m, if a very deep chlorophyll maximum was encountered then even down to 200 m) at 24 CTD stations. Water samples for CDOM absorption analysis were filtered through 0.2 µm filters and analyzed on board with a 2.5-m path length liquid waveguide capillary cell system (LWCC, WPI). The particulate and phytoplankton absorption coefficients were determined with the quantitative filter techniques using sample filtered onto glass-fiber filters and measuring them in a portable QFT integrating cavity setup QFT-ICAM following Röttgers et al. (2016). QFT data have been directly analysed on board following the method by Röttgers et al. (2016) applied to field data described in Liu et al. (in press) to derive the corresponding chlorophyll a concentrations.

c) Samples for determination of phytoplankton pigment concentrations and composition were taken from the same water samples as measured under b). These water samples were filtered on board immediately after sampling and the filters were thermally shocked in liquid nitrogen and then stored in the -80°C freezer. The samples will be brought to the AWI after arrival in Bremerhaven within a dry-ice filled box. Then these samples will be analyzed within the next three months by High Performance Liquid Chromatography Technique (HPLC) at AWI following Taylor et al. (2011).

d) Radiometric measurements to obtain apparent optical properties: At 19 daylight stations (except for station 3) we measured continuously hyperspectral upwelling radiance and downwelling irradiance with the Trios RAMSES sensors ASC-VIS and ACC-VIS, respectively, down to maximum of 130 m, adapted to the incoming sunlight. Except for the station PS113_18-1, the light frame was operated with the ship turned into the sun, avoiding shading by the ship. We stopped 30 sec to 1 min. at depths which were every 5 m up to 30 m and then every 10 m up to the maximum depth which depended on the incoming solar radiation to allow a better collection of radiometric data. Most light stations took place around local noon time or +/-4 hrs before or after but still with sufficient incoming sunlight (global radiation higher than 250 $Wm^{-2}s^{-1}$ (11:00-13:00). TRIOS RAMSES radiance and irradiance sensors were mounted on the same steel frame (in addition to the AC-s *in-situ* spectrophotometer) in downward and upward 90° direction, respectively. Another RAMSES irradiance sensor was mounted looking upwards on the Triaxus/topAWI system and operated at all deployments. The data were corrected by changes in solar irradiance, which

was measured continuously during the light stations and Triaxus deployments with another RAMSES ACC irradiance sensor on the same side of the ship. This sensor was operated always without shading by the ship. The RAMSES data were processed following NASA Ocean Optics protocols as adapted to our deployment in Taylor et al. (2011).

e) Algorithms (following e.g. Bracher et al., 2015; Chase et al., 2013; Craig et al., 2012; Bracher et al., 2009; Kostadinov et al., 2009) to extract later (back home) from the IOPs and AOPs the particulate composition, including a characterization of the phytoplankton community structure and status on photoacclimation, will be adapted to the region and maybe further developed by using the discrete water sample measurements, also for its validation.

Preliminary and expected results

We measured continuously the surface water at 11 m depth with the AC-s flow-through system from 10 May 2018 12:00 UTC to 3 June 2018 2:10 UTC and from 3 June 2018 16:30 UTC to 9 June 14:00 UTC following the cruise track. Within this time frame we sampled every 3 hours (we sampled at 2:00, 5:00, 8.00, 11:00, 14:00, 17:00, 20:00, 23:00 UTC) the same surface water and collected 202 underway samples in total. In addition, we took 143 water samples at the CTD stations (see Table 4.1). Overall, we filtered and kept at -80°C 301 pigment samples. For the same water samples as for the pigment samples we measured the particulate, phytoplankton and CDOM absorption directly on board. We took continuous profiles of IOPs (with an AC-s) and of AOPs (with the RAMSES sensors) at 21 (all except CTD stations PS113_10.2, PS113_20.1, PS113_21.1, PS113_25.1) stations (see Table 4.2). However, RAMSES data could not be collected at PS113_5.1 and PS113_6.1 because, due to high sea state, we expected too high tension on the cables. During the ten deployments of the Triaxus/topAWI (see details in the topAWI-group's cruise report) when the data collection was turned on at the system, also the hyperspectral AC-s and RAMSES irradiance sensors collected data. Unfortunately, a cable connected to the RAMSES-Triaxus sensor broke during the deployment on 27 May 2018, and at deployments on this day and the following only a limited number of profiles could be collected. At 29 May 2018 this cable was repaired, and the RAMSES-Triaxus data collection continued without any problems at the two following deployments.

Tab. 4.1: Summary of the oceanographic CTD stations sampled at discrete depths for substances of influence on optical properties. The time when the 11 m sample was taken is given. Water samples were processed for analysis of phytoplankton pigments by HPLC, colored dissolved organic matter absorption by LWCC and total particulate, non-algal and phytoplankton absorption by QFT-ICAM instruments.

Station	UTC Date	Time	Sampled Depth [m]	Lat	Lon
PS113_1-2	2018-05-10	18:37:49	11,20,30,40,65,100	-47.65	-60.71
PS113_3-2	2018-05-11	15:45:09	11,20,30,40,50,100	-44.90	-56.76
PS113_5-2	2018-05-12	15:37:38	11,20,35,50,70,100	-42.17	-52.86
PS113_6-2	2018-05-13	15:39:42	11,20,40,60,80,100	-38.88	-48.65
PS113_7-2	2018-05-14	16:06:55	11,30,60,75,90,100	-35.79	-44.78
PS113_9-2	2018-05-15	15:05:58	11,30,50,70,100,120	-33.12	-41.59
PS113_11-2	2018-05-16	15:06:03	11,30,60,90,105,130	-30.69	-39.04
PS113_13-2	2018-05-17	14:41:11	11,30,50,70,100,130	-27.06	-37.26
PS113_14-2	2018-05-18	15:06:17	11,50,75,110,130,160	-22.99	-35.34
PS113_15-1	2018-05-19	11:41:52	11,40,70,100,130,180	-19.60	-33.62
PS113_17-2	2018-05-20	14:57:41	11,40,80,110,135,185	-15.94	-31.56
PS113_18-2	2018-05-21	13:46:28	11,70,110,140,180,200	-12.53	-29.64

Station	UTC Date	Time	Sampled Depth [m]	Lat	Lon
PS113_20-1	2018-05-22	09:51:15	11,70,85,120,180,200	-9.77	-28.12
PS113_21-1	2018-05-22	19:19:42	11,50,80,110,140	-9.18	-27.80
PS113_22-2	2018-05-23	13:11:20	11,60,85,100,130,180	-6.28	-26.59
PS113_23-2	2018-05-24	13:35:38	11,30,50,65,90,150	-2.23	-25.04
PS113_25-1	2018-05-25	23:28:11	11,30,50,70,100,130	2.14	-24.98
PS113_26-2	2018-05-26	12:25:03	11,30,50,70,90,130	4.17	-24.63
PS113_27-1	2018-05-27	10:28:53	11,35,45,60,80,110	8.30	-23.52
PS113_28-1	2018-05-28	09:27:36	11,30,45,60,80,100	11.19	-22.69
PS113_29-2	2018-05-30	17:19:20	11,20,40,60,80,100	19.80	-21.15
PS113_30-2	2018-05-31	18:04:22	11,35,50,80,100,135	22.61	-20.55
PS113_31-1	2018-06-01	08:34:14	11,40,60,80,100,120	24.16	-19.81
PS113_33-1	2018-06-05	08:34:14	11,40,60,80,100,120	35.96	-13.01

Tab. 4.2: Summary of the oceanographic LIGHT stations (date and time of start in UTC; Lat = latitude, Lon= longitude) sampled where an AC-s (Wetlabs) and RAMSES upwelling radiance and downwelling irradiance sensors were measuring and lowered to the indicated maximum depth (Max). At stations PS113_5-1 and PS113_6-1 only the AC-s instrument was operated.

Station	Date	Time	Lat	Lon	Max [m]
PS113_1-1	2018-05-10	17:26	-47.66	-60.72	70
PS113_3-1	2018-05-11	14:40	-44.90	-56.75	70
PS113_5-1	2018-05-12	14:37	-42.11	-52.87	100
PS113_6-1	2018-05-13	14:32	-38.87	-48.65	100
PS113_7-1	2018-05-14	14:37	-35.79	-44.79	100
PS113_9-1	2018-05-15	13:29	-33.12	-41.58	120
PS113_11-1	2018-05-16	13:31	-30.66	-39.05	120
PS113_13-1	2018-05-17	13:28	-27.05	-37.27	70
PS113_14-1	2018-05-18	13:30	-22.98	-35.33	120
PS113_15-2	2018-05-19	11:56	-19.60	-33.62	80
PS113_17-1	2018-05-20	13:32	-15.94	-31.54	100
PS113_18-1	2018-05-21	12:31	-12.53	-29.64	80
PS113_22-1	2018-05-23	11:31	-6.29	-26.57	70
PS113_23-1	2018-05-24	12:19	-2.24	-25.01	82
PS113_26-1	2018-05-26	11:05	4.16	-24.64	90
PS113_27-2	2018-05-27	10:41	8.30	-23.52	100
PS113_28-2	2018-05-28	9:40	11.19	-22.70	100
PS113_29-1	2018-05-30	15:58	19.82	-21.15	90
PS113_30-1	2018-05-31	16:40	22.61	-20.54	90
PS113_31-2	2018-06-01	8:38	24.16	-19.81	110
PS113_33-2	2018-06-05	11:00	35.96	-13.12	130

On board we were already able to analyse some of the data. From the measurements of the QFT-ICAM particulate and phytoplankton absorption we derived a proxy for the chlorophyll concentration (see Fig. 4.1), which was generally correlated with the ship's underway system (Ferrybox) and CTD fluorescence sensor data and also corresponded to the MAPVIEWER's chlorophyll satellite data maps extracted from OLCI Sentinel-3A data.

We also compared the station QFT particulate, non-algal and phytoplankton absorption and chlorophyll data to the 1 % light depth and remote sensing reflectance data, both calculated from the RAMSES sensors' measurements. The measurements clearly showed the characteristic of different biogeochemical provinces, e.g. as defined by Longhurst (1997). Within the Southwest Atlantic shelves (south of 44°S) the highest phytoplankton biomass (indicated by chl-a concentration) with diatoms dominating the community was measured.

Here the phytoplankton was at maximum in the upper 30 m and decreased tremendously beneath which also corresponded to the shallow 1% light level (~40 m). Opposed to that from ~30°S through the South Atlantic Gyre and across the equator until ~8°N very low biomass overall was measured, especially in the upper 80 to 100 m and the chlorophyll maximum was always deep, with a maximum at Stations between 15°S-12°S. Here the chlorophyll maxima reached 140 m which corresponded also to the very deep 1 % light levels of over 150 m. Absorption spectra indicated that very small cyanobacteria (*Prochlorococcus*) dominated the community. Fig. 4.2 shows the 1 % light depth and the chlorophyll concentration of stations we sampled; details on the measured phytoplankton absorption spectra are not shown but can be provided on request.

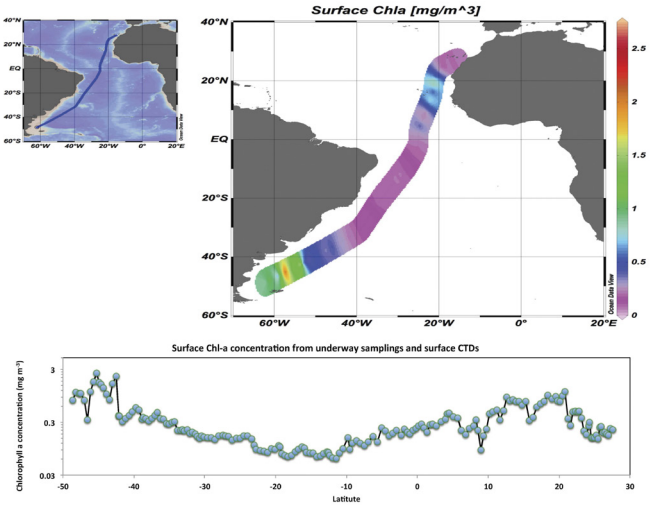

Fig. 4.1: Surface water chlorophyll-a concentration obtained from QFT-ICAM measurements of phytoplankton absorption on water samples collected from 11 m depth during PS113 until Las Palmas, Spain, using the method by Roesler and Barnard (2013) and further modified by Liu et al. (in press). Upper panel: Map showing these 11 m sample positions (left) and chlorophyll-a concentrations (right). Lower panel: Chlorophyll concentration versus latitude of the samples taken.

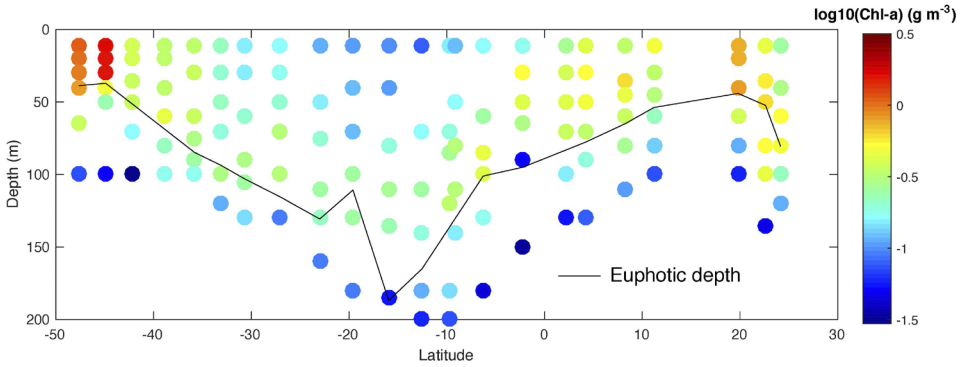

Fig. 4.2: Chlorophyll-a concentration obtained from QFT-ICAM measurements of phytoplankton absorption in water samples collected from the CTD bottles at the stations listed in Table 4.1 during PS113 until Las Palmas, Spain, using the method by Roesler and Barnard (2013) and further modified by Liu et al. (in press). The black line indicates the 1 % light depth (euphotic depth) derived from the RAMSES downwelling irradiance measurements made at the stations given given in Table 4.2.

When we are back home we need to measure the pigment samples and process all three AC-s data sets and the RAMSES-Triaxus data. For the AC-s data the adequate Milli-Q calibration measurements, temperature and salinity and scattering corrections have to be applied and spikes due to air bubbles or very large objects have to be removed. The flow-through data can be further corrected for CDOM and water absorption and attenuation measurements to

obtain particulate absorption and attenuation data. For the Triaxus and light station AC-s data on total absorption and attenuation, temporal averages (10 sec) have to be obtained to extract the correct total absorption. So we will finally obtain continuous surface water IOPs information on phytoplankton and other particulates, but also to some respect in the profiles from the AOPs determined from the radiometric data. In addition, the AOPs of reflectance and diffuse attenuation coefficient will be used for validating ocean color remote sensing data (from the Sentinel-3 (A and B) OLCI, MODIS-Aqua, MODIS-Terra, VIIRS-NPP and VIIRS-NPOESS). Those validated data sets, using the discrete samples measured in detail, will help to identify changes in phytoplankton community and its degradation products and elucidate its link to biogeochemical fluxes. The satellite information, detailed underway surface water samples, CTD, and light station profiles obtained also serve to evaluate and validate data collected with the new Triaxus/topAWI system.

Data management

Data from the analyses performed onboard directly after sampling (from the AC-s, RAMSES, LWCC and QFT-ICAM equipment) is stored at the computers and three external hard disks. These raw and partly fully analyzed data will be stored at our group storage on the AWI server. The data will be further processed and quality checked at the AWI after the expedition. Frozen filter samples brought back to AWI will be analyzed by HPLC there, where also the further data analysis will be performed. These data too will be secured/stored at our our group storage on the AWI server. The final data on particulate, phytoplankton, total and CDOM absorption and scattering and apparent optical properties will be made available after validation through the PANGAEA Data Publisher for Earth & Environmental Science. Results will be published in international journals. The metadata of the scientific measurements made during PS113 have been transmitted two months after the cruise in form of the Cruise Summary Report (CSR) to the Deutsches Ozeanographisches Datenzentrum (DOD).

References

Bracher A, Vountas M, Dinter T, Burrows JP, Röttgers R, and Peeken I (2009) Quantitative observation of cyanobacteria and diatoms from space using PhytoDOAS on SCIAMACHY data. Biogeosciences 6, 751-764.

Bracher A, Taylor M, Taylor BB, Dinter T, Röttgers R, and Steinmetz F (2015) Using empirical orthogonal functions derived from remote sensing reflectance for the prediction of phytoplankton pigment concentrations. Ocean Science 11, 139-158.

Chase A, Boss E, Zaneveld R, Bricaud A, Claustre H, Ras J, Dall'Olmo G and Westberry TK (2013) Decomposition of *in-situ* particulate absorption spectra. Methods in Oceanography 7, 110-124, 2013.

Craig SE, Jones CT, Li WKW, Lazin G, Horne E, Caverhill C, and Cullen JJ (2012) Deriving optical metrics of ecological variability from measurements of coastal ocean colour. Remote Sensing of Environment, 119, 72-83, 2012.

Kostadinov TS, Siegel DA, and Maritorena S (2009) Retrieval of the particle size distribution from satellite ocean color observations, J. Geophys. Res., doi:10.1029/2009JC005303.

Liu Y, Roettgers R, Ramírez-Pérez M, Dinter T, Steinmetz F, Noethig E-M, Hellmann S, Wiegmann S, and Bracher A (in press) Underway spectrophotometry in the Fram Strait (European Arctic Ocean): a highly resolved chlorophyll *a* data source for complementing satellite ocean color. Optics Express.

Longhurst AR (2010) Ecological geography of the sea. Academic Press.

Roesler CS, Barnard AH (2013) Optical proxy for phytoplankton biomass in the absence of photophysiology: Rethinking the absorption line height. Methods in Oceanography, 7, 79-94.

Röttgers R, Doxaran D, and Dupouy C (2016) Quantitative filter technique measurements of spectral light absorption by aquatic particles using a portable integrating cavity absorption meter (QFT-ICAM), Opt. Express, 24(2), A1-A20.

5. PRO- AND EUKARYOTIC DIVERSITY ALONG A LATITUDINAL GRADIENT IN THE ATLANTIC OCEAN

Cora Hörstmann[1], Susanne Spahic[1],
Anya Waite [1, 2] (embarked Las Palmas)

[1]AWI
[2]UniHB

Grant-No. AWI_PS113_00

Objectives/ Introduction

Global climate change is impacting a wide variety of marine ecosystems globally, and adequate quantification of the base of the marine food web is rapidly becoming urgent (Barnosky et al., 2012). Marine microbes, along with hetero-, mixo- and phototrophic eukaryotes, form the foundation of the marine food web (Sunagawa et al., 2015; Hutchins and Fu, 2017). Ocean salinity and temperature have been shown to co-vary with species distributions, suggesting that oceanographic changes can shift geographic boundaries and alter phenology and community structures from planktonic eukaryotes to higher trophic levels (Richardson and Schoeman 2004; Brown et al., 2009). Alterations caused by human induced climate change in the biogeography patterns of prokaryotic and eukaryotic microorganisms in the upper ocean could potentially impact the efficiency of C-fixation and cycling, and ultimately the export of organic carbon to the deep ocean, as microorganisms are key biogeochemical regulators (Hutchins and Fu 2017). During this cruise we want to achieve an in-depth understanding of microbial biodiversity gradients. High spatial resolution sampling enables us to map community shifts against the backdrop of physical and biochemical conditions. Through a comparison of samples taken through the ship underway seawater system and CTD-Rosette bottle sampling we test the capacity of the ship seawater system to support further high resolution sampling. We will use this dataset to test the following hypotheses concerning the ecological mechanisms controlling pro- and eukaryotic richness in the Atlantic Ocean:

H1) Richness increases with increasing productivity (more resources support higher numbers of species), and

H2) Richness increases with increasing temperature (higher temperatures increase the rates of biochemical and metabolic pathways).

H3) Stable fronts and hydrographic features, which can be surveyed quasi-synoptically at high resolution by the Triaxus towed undulating system of the AWI (topAWI), act as control mechanisms on microbial assemblages (structuring of unique microbial oceanic provinces via ecological boundary).

Work at sea

We assessed quantity and composition of marine microbes, including both eukaryotic and prokaryotic organisms, other particulates (particulate organic carbon POC and particulate organic nitrogen PON), dissolved inorganic nutrients, relative ratio of phototrophic to heterotrophic organisms and primary productivity using stable isotopes (^{13}C). Samples were collected as follows:

1) Discrete measurements of sea surface water were taken from about 11 m depth through the ship´s seawater system (teflon tubing with a membrane pump) at an interval of 3 hours.

2) Further samples were taken from the CTD rosette within the upper ocean (mostly down to 400 m depth) at 24 CTD stations. We took samples at only 11 m depth for genomic analysis, and phototrophic to heterotrophic ratios; at 3 depths for POC:PON ratios and at 6 depths for dissolved inorganic nutrient analysis.

3) During the voyage segment between Las Palmas and Bremerhaven we also sampled the ships intake via the AUTOFIM (**auto**mated **fi**ltration system for **m**arine microbes) on *Polarstern* in order to assess its applicability in parallel to genomic sampling of the underway system and CTD Rosette. All samples were filtered and frozen at -80°C for further molecular genetic analyses in the home laboratory (AWI, Bremerhaven).

Samples were further processed as followed:

a) The water from the Rosette and underway system was filtered for biogeochemical parameters including chlorophyll *a* and particulate organic carbon and nitrogen (POC/N), through 0.7 µm filters immediately after sampling and the filters were thermally shocked in liquid nitrogen and then stored in the -80°C freezer.

b) Water samples for genomic analysis were filtered through 0.2 µm Sterivex® filters within a maximum of 40 minutes after sampling. Filters were tightly closed and thermally shocked in liquid nitrogen and stored in -80°C until further analysis.

c) Water samples for dissolved inorganic nutrients were filtered through 0.22 µm syringe filters. Filtered water will be kept in -80°C until further analysis.

d) Water samples for phototrophic to heterotrophic organisms ratios were incubated in the dark prior to fixation using 0.2% PFA. Samples were thermally shocked in liquid nitrogen and stored in -80°C. Samples will be analyzed by flow cytometry in the home laboratories.

e) Primary production rate experiments were initiated by adding a known concentration of (0.05 μmol L^{-1}) of ^{13}C-bicarbonate. Inoculated polycarbonate bottles were placed in on-deck incubators where temperature regulation was maintained by a continuous surface seawater flow. Neutral density screens were used for light attenuation. Samples were incubated for 24 hours. In order to assess natural isotope abundance we incubated one litre of seawater without any addition of ^{13}C for 24 h. All experiments were terminated by filtering each bottle through a 25 mm pre-combusted GF/F filter.

All samples are brought back to the AWI after arrival in Bremerhaven packed in dry- ice filled boxes. We took samples from the surface water at 11 m depth with the AC-s flow-through system from 10 May 2018 17:00 UTC to 3 June 2018 2:10 UTC and from 3 June 2018 16:30 UTC to 8 June 23:00 UTC following the cruise track. Within this time frame we sampled every 3 hours (we sampled at 2:00, 5:00, 8.00, 11:00, 14:00, 17:00, 20:00, 23:00 UTC) the same surface water and collected 190 underway samples in total (Table 5.1). In addition, we took 143 water sample at the CTD stations (see Table 5.2). All in all we now keep samples from 215 waypoints at -80°C. Additionally we took 11 samples using the AUTOFIM for genetic analysis from 29.05.2018 to 07.06.2018 (Table 5.3).

Tab. 5.1: Summary of samples taken from ships underway system by the GENOMICS group during PS113. Water samples were further processed for analysis of genomic content, POC/PON, dissolved inorganic nutrients and phototrophic/heterotrophic ratios.

Sample No	Date [YYYY-MM-DD]	Pumping time start [UTC]	Pumping time end [UTC]	Latitude [mean]	Longitude [mean]
1	2018-05-09	12:40:00	12:50:00	-51.9819	-66.6880
2	2018-05-10	17:30:00	17:40:00	-47.6567	-60.7169
3	2018-05-10	17:45:00	17:55:00	-47.6545	-60.7162

Sample No	Date [YYYY-MM-DD]	Pumping time start [UTC]	Pumping time end [UTC]	Latitude [mean]	Longitude [mean]
4	2018-05-10	23:02:00	23:10:00	-47.0076	-59.7496
5	2018-05-11	02:04:00	02:08:00	-46.5546	-59.0908
6	2018-05-11	05:01:00	05:08:00	-46.1200	-58.4638
7	2018-05-11	08:01:00	08:08:00	-45.6882	-57.8456
8	2018-05-11	11:00:00	11:10:00	-45.2355	-57.2028
9	2018-05-11	15:30:00	16:00:00	-44.8876	-56.7500
10	2018-05-11	20:02:00	20:10:00	-44.6132	-56.3187
11	2018-05-11	23:00:00	23:05:00	-44.3231	-55.9224
12	2018-05-12	02:10:00	02:13:00	-43.8661	-55.2887
13	2018-05-12	05:01:00	05:05:00	-43.4399	-54.7021
14	2018-05-12	08:01:00	08:04:00	-42.9817	-54.0762
15	2018-05-12	11:01:00	11:05:00	-42.5174	-53.4464
16	2018-05-12	14:00:00	14:10:00	-42.1129	-52.9019
18	2018-05-12	17:00:00	17:05:00	-42.0396	-52.6649
19	2018-05-12	20:02:00	20:06:00	-41.5896	-52.2338
20	2018-05-12	23:01:00	23:05:00	-41.1725	-51.6487
21	2018-05-13	02:06:00	02:12:00	-40.6888	-51.0115
22	2018-05-13	05:00:00	05:05:00	-40.2305	-50.4122
23	2018-05-13	08:00:00	08:05:00	-39.7563	-49.7957
24	2018-05-13	11:00:00	11:07:00	-39.3193	-49.2315
26	2018-05-13	17:01:00	17:05:00	-38.7186	-48.4620
27	2018-05-13	20:00:00	20:04:00	-38.3271	-47.9641
28	2018-05-13	23:02:00	23:06:00	-37.8945	-47.4170
29	2018-05-14	02:00:00	02:05:00	-37.4686	-46.8816
30	2018-05-14	05:00:00	05:05:00	-37.0545	-46.3637
31	2018-05-14	08:00:00	08:05:00	-36.6564	-45.8685
32	2018-05-14	11:02:00	11:10:00	-36.2437	-45.3580
34	2018-05-14	20:03:00	20:09:00	-35.3924	-44.3135
35	2018-05-14	23:00:00	23:05:00	-35.0780	-43.9304
36	2018-05-15	02:00:00	02:04:00	-34.6467	-43.4075
37	2018-05-15	05:00:00	05:06:00	-34.2329	-42.9084
38	2018-05-15	08:00:00	08:09:00	-33.8340	-42.4298
39	2018-05-15	11:00:00	11:05:00	-33.4353	-41.9531
41	2018-05-15	19:58:00	20:04:00	-32.5039	-40.8487
42	2018-05-15	22:58:00	23:02:00	-32.1109	-40.3866
43	2018-05-16	02:02:00	02:11:00	-31.7151	-39.9227
44	2018-05-16	05:01:00	05:07:00	-31.3374	-39.4821
45	2018-05-16	11:01:00	11:09:00	-31.0477	-39.2437
46	2018-05-16	14:40:00	15:00:00	-30.6858	-39.0386
47	2018-05-16	20:02:00	20:07:00	-30.1043	-38.7697
48	2018-05-16	22:58:00	23:04:00	-29.5964	-38.5162
49	2018-05-17	02:00:00	02:04:00	-29.0797	-38.2598
50	2018-05-17	05:00:00	05:08:00	-28.5359	-37.9914
51	2018-05-17	08:01:00	08:09:00	-27.9944	-37.7254

Sample No	Date [YYYY-MM-DD]	Pumping time start [UTC]	Pumping time end [UTC]	Latitude [mean]	Longitude [mean]
52	2018-05-17	11:00:00	11:09:00	-27.4596	-37.4638
53	2018-05-17	14:20:00	14:45:00	-27.0628	-37.2643
54	2018-05-17	20:02:00	20:06:00	-26.1115	-36.8106
55	2018-05-17	23:00:00	23:05:00	-25.5754	-36.5531
56	2018-05-18	02:00:00	02:05:00	-25.0360	-36.2951
57	2018-05-18	05:00:00	05:04:00	-24.4920	-36.0360
58	2018-05-18	08:00:00	08:07:00	-23.9382	-35.7734
59	2018-05-18	11:00:00	11:07:00	-23.3945	-35.5167
61	2018-05-18	20:00:00	20:04:00	-22.2012	-34.9571
62	2018-05-18	23:00:00	23:05:00	-21.6641	-34.7067
63	2018-05-19	02:01:00	02:05:00	-21.1204	-34.4543
64	2018-05-19	05:00:00	05:05:00	-20.5985	-34.1894
65	2018-05-19	07:59:00	08:06:00	-20.0997	-33.9023
67	2018-05-19	17:00:00	17:05:00	-19.1142	-33.3376
68	2018-05-19	20:02:00	20:05:00	-18.7252	-33.1158
69	2018-05-19	22:58:00	23:02:00	-18.2445	-32.8422
70	2018-05-20	02:00:00	02:04:00	-17.7561	-32.5649
71	2018-05-20	05:00:00	05:07:00	-17.2685	-32.2891
72	2018-05-20	08:00:00	08:07:00	-16.7835	-32.0152
74	2018-05-20	20:00:00	20:05:00	-15.1809	-31.1156
75	2018-05-20	23:03:00	23:07:00	-14.6964	-30.8451
76	2018-05-21	02:00:00	02:05:00	-14.2184	-30.5787
77	2018-05-21	05:00:00	05:05:00	-13.7236	-30.3034
78	2018-05-21	08:00:00	08:07:00	-13.2316	-30.0306
79	2018-05-21	11:00:00	11:06:00	-12.7428	-29.7597
81	2018-05-21	17:00:00	17:06:00	-12.3800	-29.5592
82	2018-05-21	20:00:00	20:04:00	-11.9698	-29.3330
83	2018-05-21	23:02:00	23:05:00	-11.4644	-29.0544
84	2018-05-22	02:00:00	02:04:00	-10.9630	-28.7786
85	2018-05-22	05:00:00	05:08:00	-10.4447	-28.4928
87	2018-05-22	01:59:00	02:07:00	-10.9601	-28.7769
89	2018-05-22	23:00:00	23:04:00	-8.5617	-27.4641
90	2018-05-23	02:00:00	02:05:00	-8.0306	-27.1918
91	2018-05-23	05:00:00	05:08:00	-7.4643	-26.9848
92	2018-05-23	08:00:00	08:07:00	-6.9108	-26.7830
94	2018-05-23	17:00:00	17:05:00	-5.6315	-26.2791
95	2018-05-23	20:00:00	20:04:00	-5.0907	-26.0738
96	2018-05-23	23:00:00	23:04:00	-4.5495	-25.8690
97	2018-05-24	02:00:00	02:05:00	-4.0121	-25.6657
98	2018-05-24	05:00:00	05:07:00	-3.4747	-25.4624
99	2018-05-24	08:00:00	08:08:00	-2.9458	-25.2627
101	2018-05-24	17:00:00	17:04:00	-1.8416	-24.9999
102	2018-05-24	20:00:00	20:04:00	-1.4328	-24.9999
103	2018-05-24	23:01:00	23:05:00	-1.0339	-24.9998

Sample No	Date [YYYY-MM-DD]	Pumping time start [UTC]	Pumping time end [UTC]	Latitude [mean]	Longitude [mean]
104	2018-05-25	02:01:00	02:05:00	-0.6260	-24.9998
105	2018-05-25	05:03:00	05:08:00	-0.2243	-25.0000
106	2018-05-25	08:00:00	08:06:00	0.1709	-24.9998
107	2018-05-25	11:00:00	11:07:00	0.5777	-25.0000
108	2018-05-25	14:00:00	14:06:00	0.9695	-25.0000
109	2018-05-25	17:00:00	17:04:00	1.3773	-25.0000
110	2018-05-25	20:00:00	20:05:00	1.7861	-25.0001
112	2018-05-26	02:00:00	02:05:00	2.6611	-24.8905
113	2018-05-26	05:01:00	05:06:00	3.3234	-24.7780
114	2018-05-26	08:00:00	08:07:00	3.9677	-24.6685
115	2018-05-26	09:34:00	09:36:00	4.1068	-24.6536
117	2018-05-26	17:02:00	17:06:00	5.0530	-24.4489
118	2018-05-26	20:00:00	20:04:00	5.6430	-24.2809
119	2018-05-26	23:00:00	23:05:00	6.2148	-24.1182
120	2018-05-27	02:01:00	02:05:00	6.7775	-23.9578
121	2018-05-27	05:00:00	05:06:00	7.3506	-23.7943
122	2018-05-27	07:59:00	08:05:00	7.9331	-23.6279
124	2018-05-27	14:00:00	14:07:00	8.5762	-23.4438
125	2018-05-27	17:00:00	17:04:00	8.9443	-23.3382
126	2018-05-27	19:58:00	20:02:00	9.3088	-23.2339
127	2018-05-27	23:00:00	23:04:00	9.7512	-23.1068
128	2018-05-28	02:01:00	02:07:00	10.1903	-22.9804
129	2018-05-28	04:59:00	05:06:00	10.6260	-22.8553
131	2018-05-28	01:58:00	02:04:00	10.1829	-22.9827
132	2018-05-28	17:00:00	17:04:00	12.1336	-22.4260
133	2018-05-28	19:58:00	20:02:00	12.6101	-22.2934
134	2018-05-28	23:00:00	23:04:00	13.0587	-22.1683
135	2018-05-29	02:00:00	02:07:00	13.4881	-22.0484
136	2018-05-29	04:59:00	05:06:00	13.9292	-21.9251
137	2018-05-29	07:59:00	07:06:00	14.2858	-21.8250
138	2018-05-29	11:00:00	11:04:00	14.7847	-21.6852
139	2018-05-29	14:00:00	14:04:00	15.2862	-21.5501
140	2018-05-29	16:59:00	17:03:00	15.7988	-21.4991
141	2018-05-29	20:00:00	20:05:00	16.3176	-21.4545
142	2018-05-29	23:00:00	23:04:00	16.8493	-21.4085
143	2018-05-30	02:00:00	02:06:00	17.3845	-21.3622
144	2018-05-30	04:58:00	05:03:00	17.8970	-21.3176
145	2018-05-30	08:00:00	08:04:00	18.4275	-21.2713
146	2018-05-30	11:00:00	11:04:00	18.9660	-21.2223
147	2018-05-30	14:00:00	14:05:00	19.5067	-21.1747
149	2018-05-30	20:00:00	20:04:00	20.0828	-21.0909
150	2018-05-30	23:03:00	23:07:00	20.4583	-21.0187
151	2018-05-31	01:59:00	02:05:00	20.8343	-20.9463
152	2018-05-31	05:00:00	05:05:00	21.2234	-20.8709

Sample No	Date [YYYY-MM-DD]	Pumping time start [UTC]	Pumping time end [UTC]	Latitude [mean]	Longitude [mean]
153	2018-05-31	07:59:00	08:05:00	21.5890	-20.7788
154	2018-05-31	10:59:00	11:05:00	21.9533	-20.6866
155	2018-05-31	13:58:00	14:05:00	22.3164	-20.5946
157	2018-05-31	20:02:00	20:06:00	22.8231	-20.4657
158	2018-05-31	23:02:00	23:06:00	23.1546	-20.3219
159	2018-06-01	02:02:00	02:07:00	23.5045	-20.1413
160	2018-06-01	04:58:00	05:05:00	23.8477	-19.9639
161	2018-06-01	08:00:00	08:30:00	24.1560	-19.8048
162	2018-06-01	13:58:00	14:02:00	24.5187	-19.6157
163	2018-06-01	16:59:00	17:03:00	24.7294	-19.4332
164	2018-06-01	20:00:00	20:04:00	24.9400	-19.1443
165	2018-06-01	22:58:00	23:02:00	25.2093	-18.7730
166	2018-06-02	02:00:00	02:08:00	25.4924	-18.3820
167	2018-06-02	04:59:00	05:06:00	25.7691	-17.9995
168	2018-06-02	07:58:00	08:08:00	25.9240	-17.8050
169	2018-06-02	10:59:00	11:05:00	26.1639	-17.4515
170	2018-06-02	14:00:00	14:04:00	26.4556	-17.0452
171	2018-06-02	16:58:00	17:02:00	26.7279	-16.6655
172	2018-06-02	20:00:00	20:05:00	26.9814	-16.3107
173	2018-06-02	23:00:00	23:05:00	27.2534	-15.9292
174	2018-06-03	01:58:00	02:04:00	27.5335	-15.5357
175	2018-06-03	17:00:00	17:05:00	28.4609	-15.2693
176	2018-06-03	19:58:00	20:04:00	29.0054	-15.0952
177	2018-06-03	22:58:00	23:02:00	29.5775	-14.9271
178	2018-06-04	01:58:00	02:05:00	30.1411	-14.7704
179	2018-06-04	05:00:00	05:06:00	30.7125	-14.6148
180	2018-06-04	08:00:00	08:08:00	31.2828	-14.4563
181	2018-06-04	10:57:00	11:04:00	31.8410	-14.3004
182	2018-06-04	14:00:00	14:05:00	32.4155	-14.1390
183	2018-06-04	17:01:00	17:07:00	32.9894	-13.9768
184	2018-06-04	20:00:00	20:05:00	33.5460	-13.8181
185	2018-06-04	22:58:00	23:03:00	34.1041	-13.6583
186	2018-06-05	02:00:00	02:08:00	34.6886	-13.4895
187	2018-06-05	04:59:00	05:06:00	35.2651	-13.3219
188	2018-06-05	07:59:00	08:08:00	35.6811	-13.2118
190	2018-06-05	14:00:00	14:04:00	36.3358	-12.9999
191	2018-06-05	17:00:00	17:04:00	36.8960	-12.8252
192	2018-06-05	20:00:00	20:05:00	37.4676	-12.6456
193	2018-06-05	22:58:00	23:02:00	38.0254	-12.4690
194	2018-06-06	02:00:00	02:05:00	38.5887	-12.2893
195	2018-06-06	05:00:00	05:06:00	39.1568	-12.1067
196	2018-06-06	08:00:00	08:07:00	39.7293	-11.9208
197	2018-06-06	11:00:00	11:05:00	40.2923	-11.7373
198	2018-06-06	14:02:00	14:09:00	40.1462	-11.4598

Sample No	Date [YYYY-MM-DD]	Pumping time start [UTC]	Pumping time end [UTC]	Latitude [mean]	Longitude [mean]
199	2018-06-06	20:00:00	20:04:00	40.3713	-11.6751
200	2018-06-06	22:58:00	23:02:00	40.9892	-11.5070
201	2018-06-07	05:00:00	05:07:00	42.2727	-11.0773
202	2018-06-07	08:00:00	08:08:00	42.8856	-10.8698
203	2018-06-07	11:00:00	11:06:00	43.4057	-10.6918
204	2018-06-07	14:00:00	14:04:00	44.0228	-10.4619
205	2018-06-07	16:59:00	17:03:00	44.5457	-9.9485
206	2018-06-07	20:00:00	20:04:00	45.0806	-9.4187
207	2018-06-07	23:00:00	23:04:00	45.5911	-8.9087
208	2018-06-08	01:59:00	02:05:00	46.1183	-8.3770
209	2018-06-08	05:00:00	05:06:00	46.6479	-7.8359
210	2018-06-08	08:00:00	08:08:00	47.1771	-7.2882
211	2018-06-08	10:59:00	11:04:00	47.6913	-6.7268
212	2018-06-08	14:00:00	14:04:00	48.2260	-6.1865
213	2018-06-08	17:00:00	17:04:00	48.7465	-5.6314
214	2018-06-08	19:59:00	20:03:00	49.0715	-4.7971
215	2018-06-08	22:55:00	23:00:00	49.3875	-3.9478

Tab. 5.2: Summary of the oceanographic stations sampled for discrete depths by the GENOMICS group during PS113. The time when the 11m sample was taken is given. Water samples were further processed for analysis of genomic content, POC/PON, dissolved inorganic nutrients and phototrophic/heterotrophic ratios.

Station	Date [YYYY-MM-DD]	Time [UTC]	Sampled Depth [m]	Latitude	Longitude
PS113_1-2	2018-05-10	18:37:49	11,20,30,40,65,100,383	47.65	-60.71
PS113_3-2	2018-05-11	15:45:09	11,20,30,40,50,100,401	44.90	-56.76
PS113_5-2	2018-05-12	15:37:38	11,20,35,50,70,100,400	42.17	-52.86
PS113_6-2	2018-05-13	15:39:42	11,20,40,60,80,100,399	38.88	-48.65
PS113_7-2	2018-05-14	16:06:55	11,30,60,75,90,100,400	35.79	-44.78
PS113_9-2	2018-05-15	15:05:58	11,30,50,70,100,120,400	33.12	-41.59
PS113_11-2	2018-05-16	15:06:03	11,30,60,90,105,130,400	30.69	-39.04
PS113_13-2	2018-05-17	14:41:11	11,30,50,70,100,130,400	27.06	-37.26
PS113_14-2	2018-05-18	15:06:17	11,50,75,110,130,160.400	22.99	-35.34
PS113_15-1	2018-05-19	11:41:52	11,40,70,100,130,180.400	19.60	-33.62
PS113_17-2	2018-05-20	14:57:41	11,40,80,110,135,185,400	15.94	-31.56
PS113_18-2	2018-05-21	13:46:28	11,70,110,140,180,200,400	12.53	-29.64
PS113_20-1	2018-05-22	09:51:15	11,70,85,120,180,200,400,1000	-9.77	-28.12
PS113_21-1	2018-05-22	19:19:42	11,50,80,110,140,400	-9.18	-27.80
PS113_22-2	2018-05-23	13:11:20	11,60,85,100,130,180,400	-6.28	-26.59
PS113_23-2	2018-05-24	13:35:38	11,30,50,65,90,150,330	-2.23	-25.04
PS113_25-1	2018-05-25	23:28:11	11,30,50,70,100,130,400	2.14	-24.98
PS113_26-2	2018-05-26	12:25:03	11,30,50,70,90,130,400	4.17	-24.63
PS113_27-1	2018-05-27	10:28:53	11,35,45,60,80,110,400	8.30	-23.52
PS113_28-1	2018-05-28	09:27:36	11,30,45,60,80,100,400	11.19	-22.69
PS113_29-2	2018-05-30	17:19:20	11,20,40,60,80,100,400	19.80	-21.15
PS113_30-2	2018-05-31	18:04:22	11,35,50,80,100,135,400	22.61	-20.55
PS113_31-1	2018-06-01	08:34:14	11,40,60,80,100,120,400	24.16	-19.81
PS113_33-1	2018-06-05	08:34:14	11,40,60,80,100,120,200	35.96	-13.01

Tab. 5.3: Summary of the sampling stations using the AUTOFIM for further analysis of the microbial community.

Number	Date [YYYY-MM-DD]	Sample time [UTC]	Latitude	Longitude
PS113_auto1	2018-05-29	09:14:00	14.529.068	-21.756.717
PS113_auto2	2018-05-30	09:49:00	18.745.637	-21.243.131
PS113_auto3	2018-05-31	17:53:00	22.612.453	-2.054.609
PS113_auto4	2018-06-01	08:13:00	24.154.932	-19.804.921
PS113_auto5	2018-06-02	08:58:00	25.982.919	-1.770.306
PS113_auto6	2018-06-03	09:42:00	28.141.929	-15.415.056
PS113_auto7	2018-06-04	10:43:00	31.784.644	-14.316.358
PS113_auto8	2018-06-05	10:08:00	35.942.665	-13.121.325
PS113_auto10	2018-06-06	09:32:00	4.000.783	-1.182.984
PS113_auto11	2018-06-07	09:03:00	43.081.856	-10.803.035

Preliminary / expected results

All samples will be analysed (for biogeochemical parameters, primary productivity and molecular biology) in home laboratories at the AWI in Bremerhaven.

Data management

The metadata of the scientific measurements made during PS113 have been transmitted two months after the cruise in form of the Cruise Summary Report (CSR) to the Deutsches Ozeanographisches Datenzentrum (DOD). All data will be submitted to the PANGAEA Data Publisher for Earth & Environmental Science after validation.

References

Amend AS, Oliver TA, Amaral-Zettler LA, Boetius A, Fuhrman JA, Horner-Devine MC, et al. (2013) Macroecological patterns of marine bacteria on a global scale. Journal of Biogeography, 40, 800 811.

Barnosky AD, Hadly EA, Bascompte J, Berlow EL, Brown JH, Fortelius M, Getz WM, Harte J, Hastings A, Marquet PA, and Martinez ND (2012) Approaching a state shift in Earth's biosphere. Nature, 486(7401), p.52.

Brown M, Philip G, Bunge JA, Smith MC, Bissett A, Lauro FM, et al. (2009) Microbial community structure in the North Pacific ocean. ISME J, 3, 1374-1386.

Hutchins DA, Fu F (2017) Microorganisms and ocean global change. Nature microbiology, 2, 17058.

Mittelbach GG, Schemske DW, Cornell HV, Allen AP, Brown JM, Bush MB, et al. (2007) Evolution and the latitudinal diversity gradient: speciation, extinction and biogeography. Ecology letters, 10, 315-331.

Richardson AJ, Schoeman DS (2004) Climate impact on plankton ecosystems in the Northeast Atlantic. Science, 305, 1609-1612.

Sunagawa S, Coelho LP, Chaffron S, Kultima JR, Labadie K, Salazar G, et al. (2015) Structure and function of the global ocean microbiome. Science, 348, 1261359.

6. WAMOS II: RADAR-BASED MEASUREMENTS OF SURFACE WAVES AND CURRENTS

Katrin Hessner[1], Saad El Naggar[2], Wilken-Jon von Appen[3], Volker Strass[3]

[1]OWS
[2]RFL
[3]AWI

Grant-No. AWI_PS113_00

Objectives

The information about ocean surface waves and currents is of high importance for various kinds of applications, ranging from marine safety of offshore activities such as shipping, platforms, mining and fish farming to civil engineering challenges in the design of harbors and coastal protection constructions.

With the growing need of precise knowledge on waves/sea state, not only the number of wave measurements is continuously increasing, but also the number of different measurement devices. One way to remotely observe sea surface waves is by using nautical X-Band radars. These radars are generally used for ship traffic control. In the near range up to about three nautical miles these instruments are able to monitor the sea state visible in the radar as sea clutter in time and space. The observation of sea clutter requires a minimum wind speed of about 3 m/s.

During several scientific campaigns and industrial applications *sigma s6* WaMoS II® (referred to in the text as WaMoS) proved to be a powerful tool to monitor ocean waves from fixed platforms as well as from moving vessels, especially under extreme weather conditions. However, due to the different sampling strategy of radars in contrast to *in-situ* sensors, deviations of wave and current observations were reported, which question the reliability of such remote sensing technologies (Hessner, Reichert & Nieto-Borge, 2014; Hessner et al., 2017).

The WaMoS delivers information on the surface wave field with its main statistical information describing the sea state (significant wave height, peak wave period and direction, swell and wind sea conditions) as well as information of the surface current.

When validating current measurements carried out by either radar or ADCP (Acoustic Doppler Current Profiler) it needs to be taken into account that both systems might monitor the current at different depth levels. Because vertical homogeny of currents cannot always be presumed, observed deviation between those instruments might be misinterpreted. Therefore, current validations in the past were best carried out only under quasi barotropic (no significant vertical current shear) conditions (Hessner et al., 2017). This restriction makes the data validation on one hand challenging but offers on the other the potential to study the link between the surface and the subsurface currents.

To verify the reliability of the WaMoS system, a comparison was carried out with current measurements made by the vessel-mounted VM-ADCP during *Polarstern* expedition PS113 for most of the time 07.05.2018 - 11.06.2018 and between Punta Arenas and Bremerhaven. Due to the installation of the VM-ADCP in the ship's keel and the deep draft of *Polarstern*, the VM-ADCP however does not yield useful data in the water column above 17 m depth,

from where WaMoS obtains its current signals. A more direct comparison of current data will be conducted after the cruise with the velocity measurements made be the pair of up- and downward looking ADCPs mounted on Triaxus/topAWI, which reach up to the ocean surface.

Work at sea

During PS113 the accuracy and reliability of the WaMoS surface current measurements were evaluated under real time conditions, compared and the associated quality control thereupon improved. The following items were carried out:

1. The environmental limitations of the system during real operation were analyzed and assessed.
2. Influence factors such as ship speed, course changes, etc. were evaluated.
3. The system settings with respect to different environmental conditions were optimized.
4. The practical requirements and needs for the user, with respect to data display and data handling, were found out.
5. The usability of the graphical display was evaluated.
6. Comparison of WaMoS surface current data with currents measured by the vessel-mounted VM-ADCP was carried out.
7. The consistency of the WaMoS and VM-ADCP measurements with respect to synergy effects was evaluated.

During PS113 the performance of the WaMoS II was evaluated. It was found, that the radar signal of the X-Band radar used for the WaMoS measurement is significantly disturbed by the X-Band radar used for ship's navigation. These disturbances lead to significant data loss and hence to a measurement degradation as the WaMoS software rejects data analysis when the radar data flow is not continuous and of sufficient quality. This situation was not acceptable for real time operation as it resulted in long and inconsistent update rates with periods of no data output. Further the resulting data was not suitable for the long-term evaluation of current and sea parameters with other references.

After identifying the cause of the radar sampling issue the WaMoS radar data acquisition software was modified in order to allow also the acquisition of partly corrupted data (Fig. 6.1). The inspection of corrupted data showed that sectors of missing radar signals occurred but the rest of the signals contained sufficient sea clutter information. Anyway, in the standard WaMoS analyses the missing sectors lead to a distortion of the wave pattern and hence affect the general wave and current analysis. Further the signal strength varied significantly even within a radar rotation, which has a key impact on the quality control and indirect measure of the significant wave height via the signal to noise ratio.

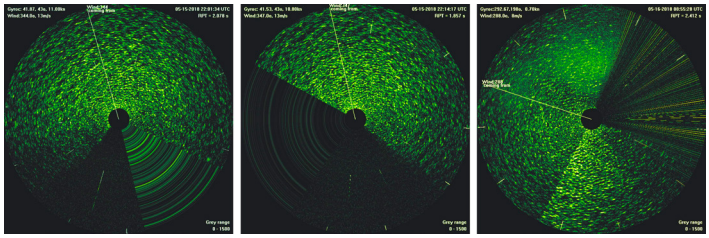

Fig. 6.1: Examples of corrupted radar images as received by the WaMoS

After identification of the problem caused by the corrupted radar data, it was possible to further adjust the WaMoS analysis software such that it can cope with partly missing radar image sectors. By implementing this modification within the operational WaMoS software, it was possible to reduce the amount of data loss significantly. The directional correction of the received radar signal in case of missing sectors allows also the use of partly corrupted data for wave and current analysis, so that the resulting wave and current data show significantly less gaps. Further tests of the resulting WaMoS data show sufficient data quality.

By updating the WaMoS software during the cruise it was possible to operate the WaMoS successfully for wave and current measurements on a continuous basis. The data inspection of retrieved wave and current showed that, apart of the raw data acquisition, also the standard quality control was affected by the interferences with the navigation radar. As a result, critical environmental conditions like no wind and rain could not be identified properly under all situations. Therefore, in a next step also the implemented standard WaMoS quality control was adjusted with respect to spikes in the radar return caused by the interferences. Here especially the identification of no wind and rain situations was addressed. This required the modification and optimization of the existing quality control and the development of new quality criteria. After testing the new algorithms also with other WaMoS data, the improved quality control was incorporated into the WaMoS software. To ensure consistent data sets for the validation, previous data sets were re-processed and the operative software was updated during the cruise. During the cruise different current regimes were passed (Fig. 6.2). Regions with highest current speeds up to 2 m/s were observed at the beginning.

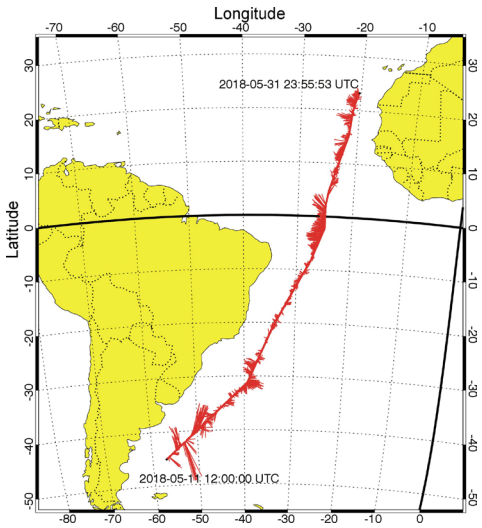

Fig. 6.2: Cruise track with stick plot indicating the surface currents observed by WaMoS during PS113 (May data only)

Preliminary results

First analysis proved the successful performance. Periods of environmental limitations of the system performance were identified and corresponding data sets were marked successfully. First analysis of the May data set show that about 80 % of the acquired data (9727) pass the quality control and can be regarded reliable. About 10 % show data with significantly reduced quality and the residual 10 % do not contain sufficient radar signals for processing. Qualitative comparisons yield that the identification of insufficient data (IQ > 0) agreed well with low wind and rain events (see Fig. 6.3). The validation of the wave parameters was not possible as no sufficient reference data was available during the cruise.

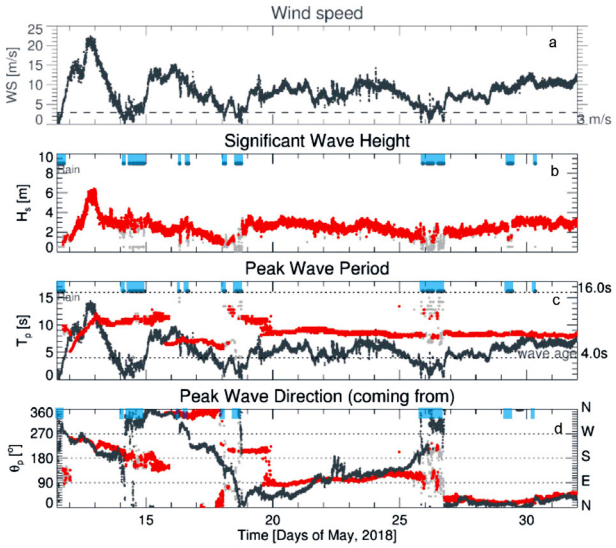

Fig. 6.3: Time series of the WaMoS sea state parameters (b, c, d), where the red dots indicate reliable data which pass the internal quality control with IQ = 0 and light grey dots refer to unreliable data due to insufficient sea clutter with IQ > 0. The dark grey data refer to onboard wind measurements (a, c, d): wind speed (top panel: a), wave age based on wind speed (middle panel, c) and wind direction (bottom panel, d). Detected rain events are marked blue.

During the cruise the results of the WaMoS surface current measurements were compared with the VM-ADCP measurements (see Fig. 6.4). These qualitative and quantitative comparisons of the measurements demonstrated the quality and reliability of the WaMoS measurement. The implemented new quality control successfully mark data with unreliable results, characterized by unrealistic variations (grey).

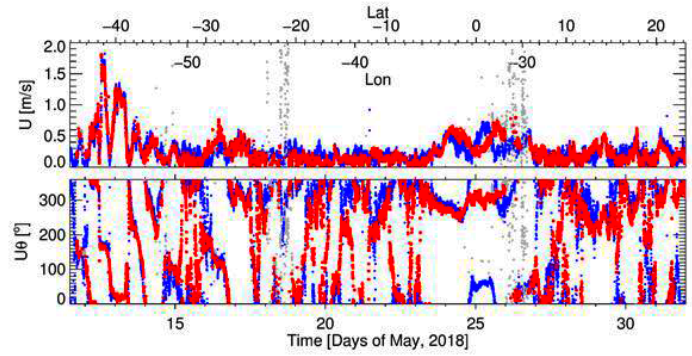

Fig. 6.4: Time series of the current speed (top panel) and current direction (going to) (bottom panel) as derived from WaMoS (red) and VM-ADCP (blue). The grey values indicate WaMoS data marked as unreliable (IQ>0).

To estimate the WaMoS current quality, these data sets were statistically compared with VM-ADCP results of the upper bins of the water column. The corresponding results for the mean ADCP measure for the upper 5 bins (an average between 17 m and 37 m) for May 2018 are shown in Fig. 6.5. All statistical estimates like correlation coefficient, bias and standard deviation of the data are in acceptable range. Note that the data obtained during the period of crossing the regime of the equatorial undercurrent was excluded, because during this period the surface and subsurface currents are physically different and thus the two platforms cannot be expected yielding measurements that correlate with each other. For the other periods both

current components reveal with 0.94 and 0.97 a very high correlation. Also bias and standard deviation of the difference are below 0.1 m/s and confirm the agreement during the times when the upper water column can be assumed to be comparable and deviations due to vertical and horizontal current shears can be neglected to first order.

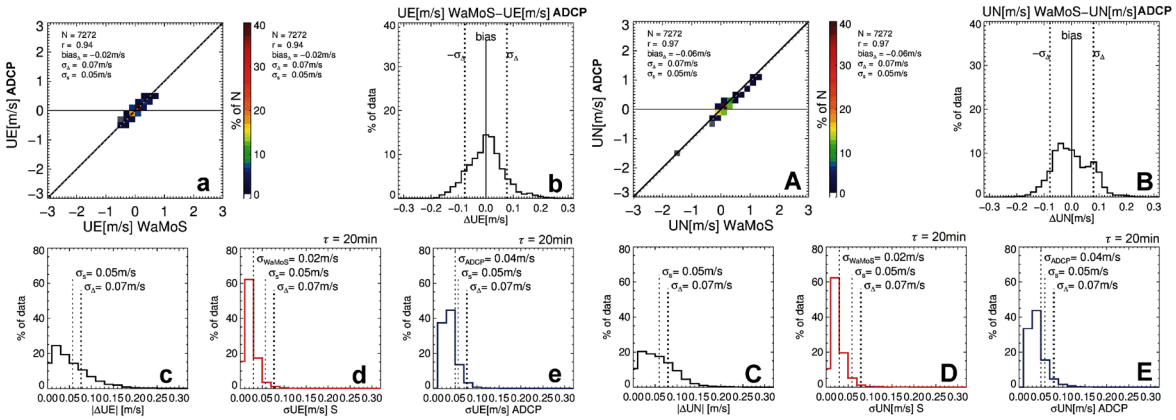

Fig. 6.5: Correlation between WaMos surface current and the reference current (mean of the upper 5 bins of the vessel-mounted ADCP) during PS113. Left: Correlation results of the East-West component UE (a-e), Right: for the North-South component UN of the current (A-E). For both current components, the correlation (UE:a, UN:A), histogram of the deviation (UE:b, UN:B), histogram of the absolute deviation (UE:c, UN:C) , and corresponding variation of WaMoS (red, UE: d, UN: D) and ADCP (blue, UE: d, UN: E). N gives the number of data pairs, r the correlation coefficient, standard deviation. Note that the period when crossing the regime of the equatorial under current was excluded, because during this period the surface (WaMoS) and subsurface (ADCP) currents represent different oceanographic regimes and therefore are not comparable.

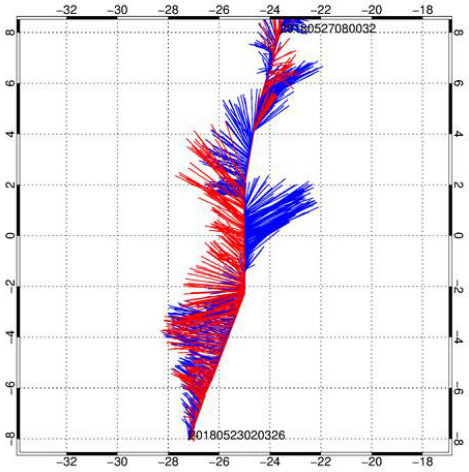

Fig. 6.6: Stick plot of the current field passing the equatorial current system. Red refers to the surface current observed by WaMoS, and blue to the subsurface current obtained by the VM-ADCP.

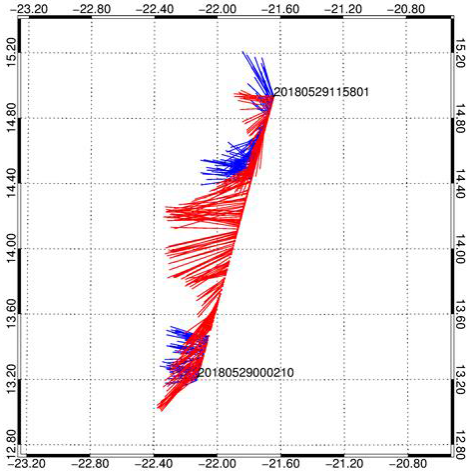

Fig. 6.7: Stick plot of the current near the Cape Verde islands. Red refers to the surface current observed by WaMoS, and blue to the subsurface current obtained by the VM-ADCP, which however was switched off during the middle of the shown period.

In areas with vertically sheared currents, like at the equator (see Fig. 6.6), additional valuable information on the dynamics in the surface ocean was provided by the WaMoS system. Another advantage of the WaMoS system is that it delivers data also when ADCP measurements are not available. For example, in the up-welling area near the Cape Verde islands a westward current filament directed offshore from the northwest African coast was observed with WaMoS while the VM-ADCP was switched off, as in the Spanish economic zone around the Canary Islands, in order of avoiding acoustic disturbances of marine life whenever possible.

Data management

The metadata of the scientific measurements made during PS113 have been transmitted two months after the cruise in form of the Cruise Summary Report (CSR) to the Deutsches Ozeanographisches Datenzentrum (DOD). WaMoS data has been observed only outside the exclusive economic zones (200-mile zones) in the period of May 11th - June 10th. Data is available with an average update rate of 2.6 minutes.

The WaMoS data set consist of different data sets, including time series of statistical sea state and surface current data as well as frequency spectra of the sea state. Corresponding metadata with respect to acquisition time (UTC) and GPS position (Latitude, Longitude), water depth and wind are either included or stored separately. All WaMoS data are stored at OceanWaveS GmbH and available on request. The quality controlled surface current measurements and sea state information will be submitted to the PANGAEA Data Publisher for Earth & Environmental Science.

References

Alpers WR, Ross DB, Rufenach CL (1981) On the detectability of ocean surface waves by real and synthetic aperture radar. J. Geophys. Res. , 86 (C7), 6481-6498.

Bitner -Gregersen EM, Hagen Ø (1990) Uncertainties in Data for the Offshore Environment. Structural Safety, Vol. 7, No. 1, 11 -34.

Hessner K (2007) WaMoS II - WAVE ANALYSIS METHOD, LIMITATIONS, AND DEFINITIONS OceanWaveS GmbH.

Hessner KG, El Naggar S, Strass V, Krägefsky S, Witte H (2017) Evaluation of X-band MR surface and ADCP subsurface currents obtained onboard the German research vessel Polarstern during ANT-XXXI expedition 2015/16. Oceans 2017.Anchorage, USA.

Hessner, KG, Reichert K, Nieto Borge JC (2014) Accuracies and error statistics for measured - Area covering X- band radar wave measurements vs point measurements. OCEANS'14 MTS/IEEE. St. Johns.

Keller WC, Wright, JW (1975) Microwave scattering and the straining of wind-generated waves. Radio science, 10(2), 139-147.

Lee P, Barte J, Beach K, Hindman C (1995) X-Band microwave backscattering from ocean waves. J. Geophys. Res., 100(C2), 2591-2611.

Plant W (1990) Bragg Scattering of Electromagnetic Waves from the Air/Sea Interface. In G. G. Plant, Surface Waves and Fluxes: Current Thory and Remote Sensing (pp. 41-108). Kluwer Academic Publishers.

Wenzel LB (1990) Electromagnetic scattering from the sea at low grazing angles. In G. L. Geernaert, Surface Waves and Fluxes: Current Theory and Remote Sensing.(pp. 41-108). Kluwer Academic Publishers.

7. ATMOSPHERIC MEASUREMENTS OF AEROSOLS AND CLOUDS WITH A MOBILE SEA FACILITY: OCEANET

Andreas Macke (not on board)[1], Ronny Engelmann (not on board)[1], Hartwig Deneke (not on board)[1], Martin Radenz[1], Cristofer Jimenez[1], Zhenping Yin[1]

[1]TROPOS

Grant-No. AWI_PS113_01

Objectives

The OCEANET-ATMOSPHERE project delivers valuable atmospheric measurement datasets over the oceans – in regions of the world that are not easily accessible. For the last 8 years, a container-based platform has been operated regularly on board *Polarstern* to obtain measurements and to contrast atmospheric processes between the anthropogenic polluted northern hemisphere and the rather pristine southern hemisphere.

The OCEANET container houses several remote-sensing instruments. The primary instrument is a semi-autonomous multiwavelength polarization Raman lidar developed at TROPOS. It is able to measure profiles of the backscattering coefficient at three wavelengths, of the extinction coefficient and of the depolarization ratio at two wavelengths as well as of the water-vapour mixing ratio.

Aerosol particle optical properties can be determined directly and serve as input for height-resolved inversion methods to estimate the main microphysical properties (e.g. size distribution) at any measured height. Thus, lofted free-tropospheric aerosol layers can be characterized separately from the marine boundary layer. Typical known free-tropospheric aerosols are anthropogenic emissions from North America, dust from the Saharan region or smoke from biomass burning in Central Africa. These aerosols can be lifted up above land and are transported over the Atlantic Ocean for several days. During this transport aerosols influence the radiation budget of the Earth. Thus, the height-resolved information as derived from lidar is a crucial input for radiative transfer calculations to determine the direct aerosol radiative effect more precisely. In addition, the height-resolved measurements offer the opportunity to determine the extent of simultaneously occurring clouds, as well as the cloud's thermodynamic state of phase (liquid or solid) to investigate aerosol-cloud interactions and to determine the aerosol indirect radiative effect.

The second major instrument is a microwave radiometer (MWR, type: HATPRO). It measures brightness temperatures in the microwave region and uses absorption bands of water vapor and oxygen to retrieve temperature profiles and humidity profiles up to 10 km altitude. Humidity profiles were used to derive integrated water vapour (IWV) and the liquid water path (LWP). In combination with the variability of the downward radiative quantities these time series make it possible to observe small scale atmospheric structures and cloud inhomogeneity.

A shadow band radiometer is located on the container roof as well. This radiometer measures the spectral and broadband down-welling radiation (0.3-1.6 micrometer range) from the upper hemisphere. Thanks to its rotating shadow band, which blocks the direct sun when scanning over the receiver surface, the global, diffuse and direct radiation were observed.

Furthermore a prototype of an automated motion stabilized sun photometer (type: CE318-T) was tested during PS113. It will offer the opportunity to apply more sophisticated retrievals due to its 9 channels, motion-corrected scanning capabilities and an anti-sea spray system.

Additionally a scalable automatic weather station (SCAWS) from the DWD measures standard parameters such as temperature, pressure, humidity, and radiation (solar and infrared) on a 1-s time basis.

Work at sea

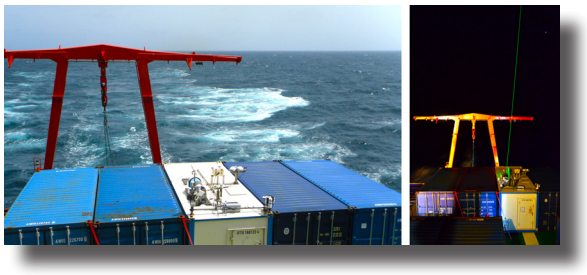

Fig. 7.1: Location of the OCEANET Container on the helicopter deck

The instrument setup and initial calibration started during port call at Punta Arenas on May 08 and was finished during the first day at sea. The container was located on the helicopter deck (Fig. 7.1) because the location at the aft of the vessel is less exposed to wind and sea spray. All the observations were taken en-route and did not depend on any station time. Regular maintenance procedures included daily cleaning of the radiation sensors and the All-Sky-Camera dome. The lidar window was also cleaned on a regular basis depending on obvious sea-spray or dust contamination. At high sun elevations between May 25 and June 6, the lidar system had to be turned off manually to protect the receivers. The measurements were monitored in real time and changes on the lidar optical receiver setup were done periodically to ensure high data quality.

Expected and preliminary results

During the cruise, covering a mostly meridional cross section from 53°S to 55°N, a huge variety of atmospheric conditions were observed. An overview of observed aerosol optical depth (AOD) and integrated water vapour (IWV) as observed by the Cimel sun photometer is shown in Fig. 7.2.

The cruise started with frequent occurrence of clouds at all heights from the boundary layer to the tropopause. From May 12 to 15, despite occasionally gale force winds, only boundary layer and cirrus clouds were present. During short cloud-free periods no distinct aerosol layers could be observed in the free troposphere. On May 16 again a multi-layered cloud system was present.

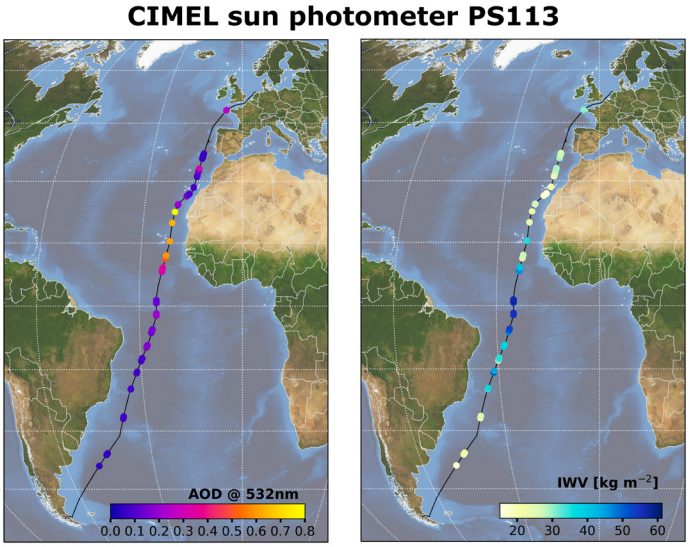

Fig. 7.2: Aerosol optical depth (left) and integrated water vapour (right) as retrieved from the CIMEL measurements

From the morning of the 17th to the evening of the following day, the sky was clear bevor a frontal like cloud system brought some rain. It became obvious during this time that the microwave radiometer must have experienced some damage during the transport or the strong wind period, as the temperature stabilization of the receivers failed. Hence, the measured brightness temperatures experience a strong drift and most likely are not usable in retrievals.

Between May 19 and the equator crossing on May 25 mostly low level layer clouds of various depths were observed, occasionally interrupted by short showers. Around May 20 aerosol load was very low with an AOD below 0.1. A first thin aerosol layer was observed between 2 and 4 km on the 24th and morning of the 25th of May. Low particle depolarization and high lidar ratio values suggest a mixture of smoke and mineral dust. Crossing the ITC during the afternoon and the following day, frequent showers occurred. In the tropics IWV values up to 55 kg m^{-2} were observed.

The dust outflow of the Saharan desert was reached in the early hours of the May 27. A dust plume between 1.5 and 4.5 km could be observed for the following 6 days (Fig. 7.3), extending roughly from 6°N 24°W to 23°N 20°W with an AOD of up to 0.7. Extinction coefficients were up to 500 Mm^{-1} (532 nm and 355 nm) with a lidar ratio around 50 and particle depolarization of 25 % (both 532 nm).

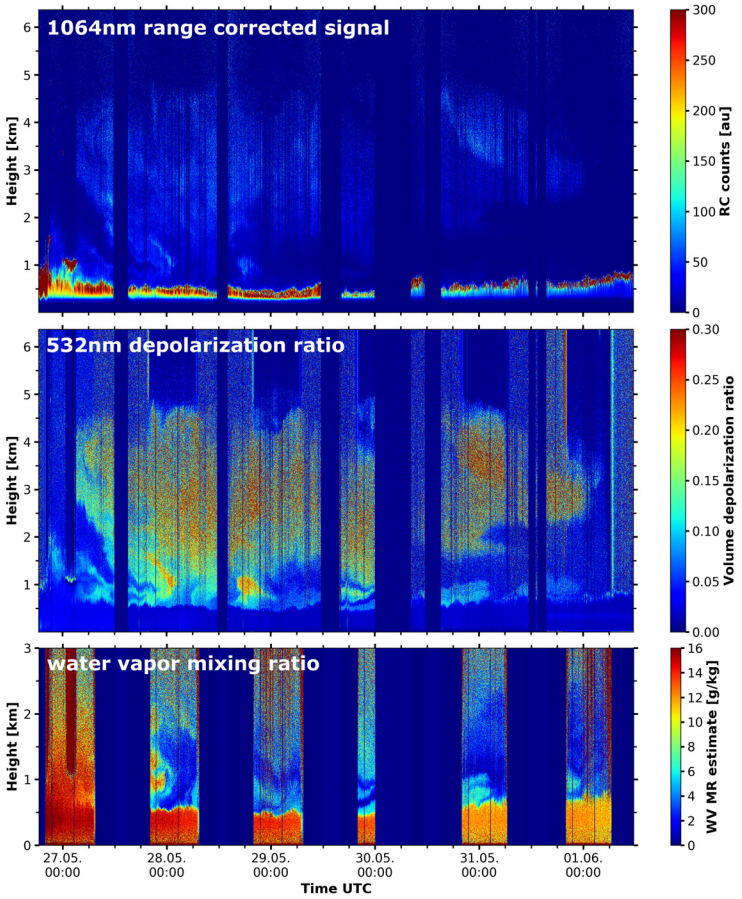

Fig. 7.3: PollyXT lidar observation for the period of the dust plume

Approaching the Canary Islands, frequent boundary layer clouds with base heights around 500m hampered the aerosol observations again. Short cloud free periods in the evening of June 2 and the morning of June 3 revealed marine dominated aerosol conditions. In the night of June 4 mid and high level clouds were observed. Between June 5 and 8 stratus clouds with low cloud base height prohibited any meaningful lidar observations.

Upon entry of the English Channel in the evening of June 8, multi-layer clouds were observed and plumes of continental pollution became the dominant aerosol type.

Data management

The metadata of the scientific measurements made during PS113 have been transmitted two months after the cruise in form of the Cruise Summary Report (CSR) to the Deutsches Ozeanographisches Datenzentrum (DOD). All data processing will be carried out at TROPOS in Leipzig. The primary address for the data access should therefore be TROPOS but as soon as the data are available they can be used by other cruise participants after request. Additionally, it is foreseen to upload the quality-checked data to PANGAEA Data Publisher for Earth & Environmental Science. However, this data processing and upload procedure might take a few months.

8. OPTICAL MEASUREMENTS OF AEROSOL, WATER VAPOR AND CLOUD PROPERTIES

Jessica Vial[1], Stefan Kinne[1] (not on board) [1] MPI-M

Grant-No.: AWI_PS113_02

Objectives

Owing to their modulation of the Earth's radiation budget, of the surface energy balance and of the tropospheric diabatic heating, clouds and aerosols have the potential to affect many aspects of climate (e.g., climate sensitivity, equator-to-poles energy transports, tropical and extratropical circulations, precipitation). While this has been recognized for a long time, the representation of clouds, aerosols and their radiative processes still remains one of the most sensitive aspects of climate modeling (i.e., small changes in cloud/aerosol parameters can lead to large impacts on many aspects of the simulated climate). For a better understanding of clouds, aerosols and their interactions with radiation, and to evaluate and improve their representation in climate models, observations are required. They are required not only at the climate scale (e.g., years-to-decades of global coverage from satellites), but also at finer spatial and temporal scales for process studies. Our objective aboard *Polarstern* on the PS113 transatlantic transect was to collect high-frequency data of clouds, aerosols and water vapor, which in conjunction with meteorological data on the ship, will provide valuable insights into the small scale processes related to aerosols and water in the atmosphere.

8.1 Column-integrated measurements of aerosols and water vapor

Work at sea

A MICROTOPS sun-photometer had been provided by NASA to collect data of aerosol properties and water vapor content. The data was submitted and quality checked by the Marine Aerosol Network (MAN) as part of the Aerosol Robotic Network (AeroNet, Smirnov et al., 2009). The small hand-held instrument (Fig. 8.1) measures the direct solar radiation (during the day when the solar disk is not obscured by clouds. It is combined with a GPS sensor to estimate the intensity at the top of the atmosphere. Incoming solar radiation measured on the ship is reduced by absorption and scattering. Based on associated differences in radiation, properties of atmospheric aerosols and water vapor content along the transect are derived.

The MICROTOPS measurements are a contribution to the typically sparse network over remote waters (Fig. 8.1). They help to better understand the Earth radiation budget, e.g. the measurements are used to update the present-day aerosol climatology of MPI-M (MAC, Kinne et al., 2013). This climatology is the basis for the simple plumes parameterization MACv2.0-SP1.0 for aerosol optical properties for usage in CMIP6 models (Stevens et al., 2016; Fiedler et al., 2017). The MICROTOPS measurements from this expedition could be further used for validation and development of satellite products and atmospheric models as well as inter-disciplinary studies (such as ocean optics and phytoplankton productivity carried by the PhytoOptics group also aboard PS113; see Chapter 4).

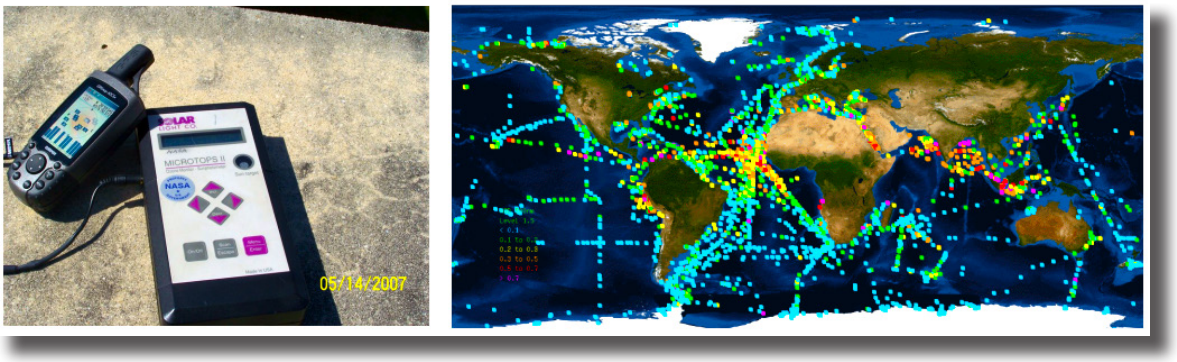

Fig. 8.1: (left) MICROTOPS instrument, (right) network of past observations within the Marine Aerosol Network (MAN, http:/aeronet.gsfc.nasa.gov/new_web/maritime_aerosol_network.html)

Preliminary results

The focus was on three specific aerosol properties: The AOD at 550 nm, the Angstrom parameter and the water vapor content, to capture aerosol amount, aerosol size and the atmospheric water vapor content, respectively. The MICROTOPS measurements are made at five solar wavelengths: 380, 440, 670, 870 and 940 nm. The first four wavelengths were used to extract the AOD for aerosol amount. The AOD at 550 nm, a value commonly used in global modeling and satellite remote sensing, is not directly measured but interpolated based on the spectral dependence of the AOD. The Angstrom parameter, defined as the negative slope in the log(wavelength)/log(AOD) space, provides information on the dominant aerosol size, such that values larger than 1.0 indicate dominant contributions by smaller aerosols (e.g. from pollution, black carbon and organic compounds), while values smaller than 0.5 indicate the dominant influence by larger aerosols (e.g. mineral dust and sea-salt). The last two wavelengths (water vapor absorbs at 940 nm but not at 870 nm) are used to extract the water vapor content in the atmosphere. Latitudinal cross-sections from the PS113 transit for these three properties are presented in Fig. 8.2. Due to the frequent occurrence of clouds at the beginning of the cruise, the measurements only started on 15 May 2018.

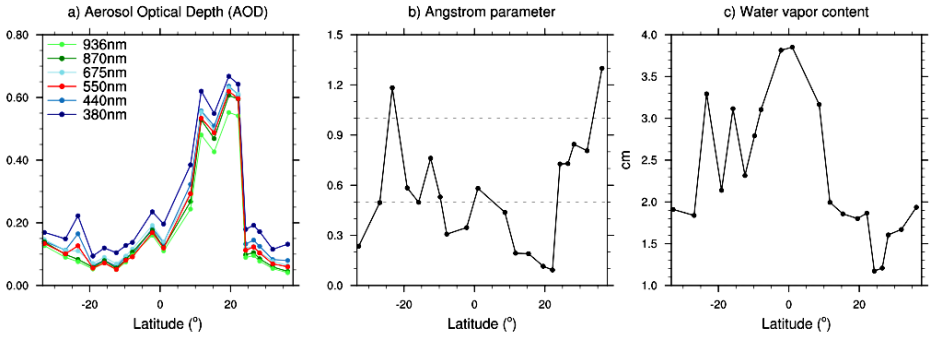

Fig. 8.2: Atlantic transect of aerosol properties and water vapor content directly sampled or derived from the MICROTOPS measurements. Shown are daily means for (a) AOD at different wavelengths, (b) the Angstrom parameter for 380 nm/870 nm and (c) column-integrated water vapor content. All data have been quality controlled.

The AOD latitudinal cross-section (Fig. 8.2a) is dominated by a strong dust event off Northwest Africa between 10°N and 20°N. The low Angstrom parameter in this region is indicative of large mineral dust sizes (Fig. 8.2b). Elsewhere along the transit, relatively clean aerosol conditions could be observed (low AODs at 500 nm, < 0.1). However, this was also sometimes associated with a relatively high Angstrom parameter, for instance, near 20°S (slightly south of Rio de Janeiro, on the 18th) and north of 20°N (north of Cape Verde, from 1st June). In the southern hemisphere, these high Angstrom values could be associated with a mixture of anthropogenic and natural organic aerosols emitted over South America, which are then transported by the winds over the ocean. When we approached the Canary Islands, however, anthropogenic aerosols were perhaps more likely associated with pollution.

The water vapor content along the transit is shown in Fig. 8.2c. The data shows clearly larger values in the tropics than in the subtropics and mid-latitudes. This is partly because of the strong dependence of the saturation vapor pressure on temperature and also because of the large-scale circulation that is subsiding (and thus drying) over the vast subtropical regions. In addition, the increase from lower water vapor at higher latitudes to larger values near the equator is non-monotonic and often controlled by different air-mass transports in the subtropics (e.g., advection of dry continental air by the trade winds off northwestern Africa) and in the mid-latitudes (e.g., warm conveyor belts in the southern hemisphere mid-latitude cyclones).

8.2 Measurements of cloud cover, structure and cloud base altitude

Work at sea

The ‘Pinocchio’ cloud camera system from MPI-M (Fig. 8.3) had been operated from 10 May 2018 until 8 June 2018. It contains two cameras, one for visible and one for near-infrared radiation. The system was installed on the observation deck at the starboard reeling, and was connected to energy supply and a computer in the research lab on *Polarstern’s* A level deck. Pointed towards the sky, it automatically recorded images of the sky and cloud scenes every 10 seconds. While the hemispheric visible camera was only used to get a general overview of the sky during daytime, images from the thermal camera were processed to derive cloud properties.

Before the cruise, the thermal camera was calibrated in laboratory in order to determine the brightness temperature for every pixel of an infrared image (Fig. 3). With a field of view of 45°, the calibrated thermal camera provides temperature images of the sky and clouds. Thus, it cannot only sample cloud cover but also cloud field organization and cloud base altitudes. The derivation of these cloud properties is subject of ongoing research at MPI-M.

As the thermal camera senses in the near IR-window (8.5-11.0µm region), where trace-gas absorption is usually small, first estimates of cloud base altitudes were derived by assuming a close to dry-adiabatic lapse rate with altitude (e.g., 8 to 9°C colder than the surface temperature corresponds to a cloud-base altitude near 1,000 m). This assumption, however, fails when water vapor content increases (as in the tropics) as now the water continuum absorption and moist-adiabatic adjustment warm the clear-sky background and so smaller effective lapse rates need to be applied.

Aboard PS113, the impact of water vapor on the background temperature was assessed and a new approach was employed to determine the cloud base altitudes. Additionally, cloud cover at pre-defined altitudes were computed and compared with similar cloud statistics derived from the lidar instrument deployed and operated by the TROPOS group and the ship’s ceilometer.

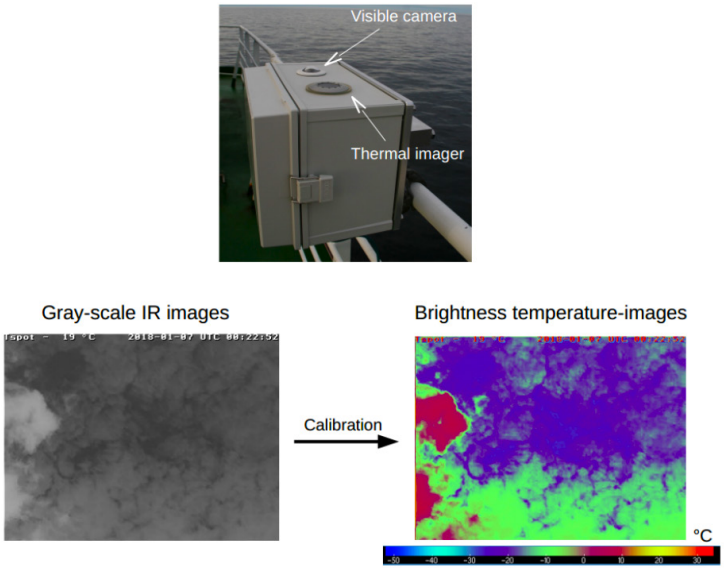

Fig. 8.3: Photo of the 'Pinocchio' cloud camera system (top). Example of the infrared images before calibration (bottom left) and temperature images after calibration (bottom right).

Preliminary results

To investigate the impact of the water vapor on the background (sky) temperature, the minimum temperature from thermal camera images were computed at times of MICROTOPS sun-photometer samples (which require un-obstructed views of the solar disk). Using the temperature profile from radiosondes (launched daily from the ship at 11:00 UTC), the maximum radiative height of the sky seen by the camera could also be estimated. This provides a useful information, as this height can also be seen as setting the upper limit for cloud detection; above it cloud detection cannot be achieved due to the lack of a thermal contrast between the radiative temperatures of the cloud and of the surrounding sky. Finally, a mean temperature lapse rate was estimated (also at times of sun-photometer measurements), based on the difference between the near-surface temperature (from the ship's sensor at ~30m) and the minimum temperature of the thermal image divided by the estimated radiative height of the sky. In Fig. 8.4, the near-surface temperature, minimum temperature of the thermal image, radiative height of the sky and lapse rate are plotted against latitude (top row) and the water vapor content measured with the MICROTOPS sun-photometer (bottom row).

The near-surface and radiative sky temperatures are linearly dependent on the atmospheric water vapor content, with increased temperatures as the atmosphere gets moister in the tropics. As a result, the radiative height of the sky - and with it, the maximum height at which clouds can be detected with the thermal camera - is also dependent on the atmospheric water vapor. At high latitudes and low moisture content, cloud detection can be done roughly up to 8 km, while in the moister tropics only clouds up to 4 km can be detected. Interestingly, the lapse rate dependence on water vapor does not appear as strong as it was expected, despite a clear dependence on latitude that suggests (from the second order polynomial fit in Fig. 8.4d) a close to dry-adiabatic lapse rate (between 8 and 9°C/km) at high latitudes and a reduced lapse rate (to about 5°C/km) in the tropics.

For the cloud altitude data processing the radio-sounded temperature profile was used to estimate the cloud cover at 6 different altitudes in the lower troposphere: 0.5, 1, 1.5, 2, 3 and 5km. Cloud detection was not done above 5 km due to the upper limit sets by the radiative sky height (Fig. 8.4c, g). Results of this altitude associated cloud cover for the entire transit are presented in hourly averages in Fig. 8.5a. The cloud base altitudes related cloud cover values are plotted on top of each other as cloud cover (for a ground observer) is increasing with altitude.

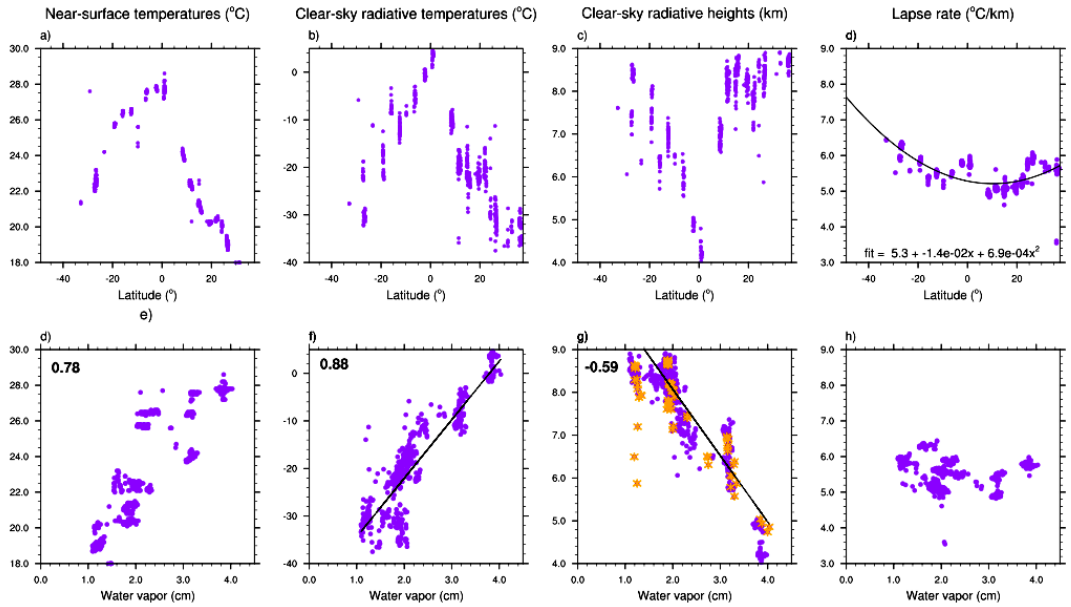

Fig. 8.4: Thermal properties of the atmosphere at times of MICROTOPS sun-photometer measurements, plotted as a function of latitude (top row) and column-integrated water vapor content (bottom row). Shown are (a, d) the near-surface temperatures from the DSHIP database, (b, f) the minimum temperatures of the thermal images, (c, g) the corresponding radiative heights estimated from radiosounding at 11:00 UTC - the orange markers in (g) are at times close to radiosounding measurements (plus or minus 30 minutes) and (d, h) the estimated lapse rates.

The cruise started with clouds at different altitudes in association with some mid-latitude cyclones and fronts that were crossed along our route (up to about 20°S). Some days during this period the sky was completely overcast, mainly by clouds with bases ranging between 1 and 2 km (from frontal systems). In the southern subtropics, the cloud cover was mainly dominated by low-level clouds with bases between 500 m and 1 km, which is consistent with the predominance of stratocumulus and shallow cumulus clouds that are typically found in this region. Entering the central tropics (with the ITCZ slightly north of the equator), cloud bases at relatively low levels were also detected. This could be the signature of high water vapor content in the lower troposphere lowering the lifting condensation level where clouds typically start to form. Finally, in the northern subtropics the cloud cover was reduced, especially during the Saharan dust event where the trade winds also carried very dry continental air from northern parts of Africa (Fig. 2c). It is however surprising that during that time the thermal camera essentially captured clouds with bases between 3 and 5 km. A more in-depth quality check of the data should be done at MPI-M after the cruise.

Comparison is made now with similar cloud statistics derived from the lidar (Fig. 8.5b, with data available only up to about 15°S at the time of writing up this report) and ceilometer (Fig. 8.5c) instruments. In general, the detection of total cloud cover (up to 5 km) is often similar between the three instruments, but large differences arise regarding the vertical distribution of cloud bases (e.g., within the latitudinal windows 15°-25°S, 30°-35°S). Nevertheless, comparable cloud vertical distributions can also be seen at many occurrences. Just to give one example, at the beginning of the cruise all three instruments were able to detect the same cloud cover with cloud bases at 5 km.

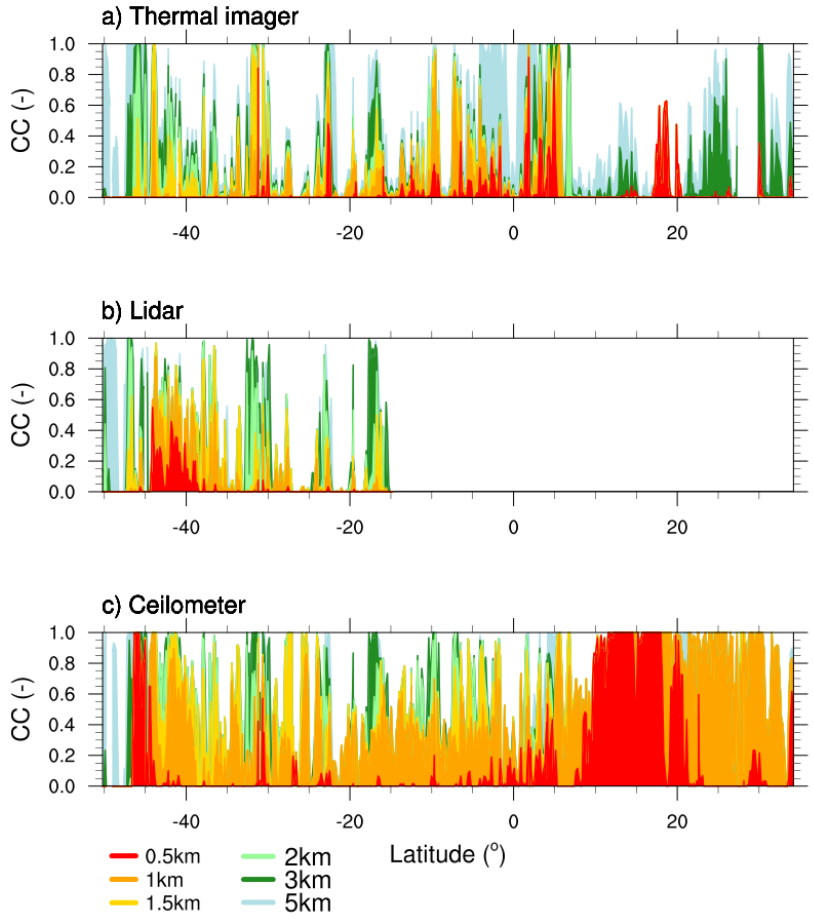

Fig. 8.5: Hourly averaged cloud cover for all pre-defined altitudes (0.5, 1, 1.5, 2, 3 and 5 km) as function of latitude from (a) the thermal camera images, (b) the active lidar detection (TROPOS) and (c) active ceilometer detection (part of the ship instrumentation).

For the thermal camera, this cloud base altitude related cloud cover distribution is only weakly sensitive to the background temperature profile (or lapse rate) that is used to estimate the cloud base altitudes (not shown). Therefore, the differences between the instruments are believed to be mainly due to different sensor capabilities and sensitivities to particles and water in the atmosphere. For instance, the ceilometer, which is also sensitive to the presence of aerosol particles, was probably detecting the dust layer rather than clouds between 10° and 25°N (during the Saharan dust event). Further analysis could also be done to determine how these cloud detection similarities/differences depend on weather regimes (e.g., mid-latitude cyclones vs. stratocumulus/shallow cumulus regions).

Data management

All sampled sun-photometer AOD data were quality controlled and are accessible along with derived detail on AOD attribution to aerosol size classes plus the water vapor data on NASA marine aerosol web: https://aeronet.gsfc.nasa.gov/new_web/cruises_new/Polarstern_18_0.html. The camera visible and thermal images of the sky (usually captured every 10 second) are stored on a local server at the MPI-Meteorology and are made available on request by sending an e-mail to stefan.kinne@mpimet.mpg.de. The metadata of the scientific measurements made during PS113 have been transmitted two months after the cruise in form of the Cruise Summary Report (CSR) to the Deutsches Ozeanographisches Datenzentrum (DOD).

References

Fiedler S, Stevens B, and Mauritsen T (2017) On the sensitivity of anthropogenic aerosol forcing to atmospheric variability and parameterizing a Twomey effect. Journal of Advances in Modeling Earth Systems, 9, 1325–1341, doi:10.1002/2017MS000932.R

Kinne S, O'Donnel D, Stier P, Kloster S, Zhang K, Schmidt H, Rast S, Giorgetta M, Eck T F, Stevens B (2013) MAC-v1: A new global aerosol climatology for climate studies. Journal of Advances in Modeling Earth Systems, 5 (4), 704–740, doi: 10.1002/jame.20035.

Smirnov et al. (2009) Maritime Aerosol Network as a component of Aerosol Robotic Network, J. Geophys. Res., 114, D06204, doi:10.1029/2008JD011257.

Stevens B, Fiedler S, Kinne S, Peters K, Rast S, Müsse J, Smith S J, Mauritsen T (2016) Simple Plumes: A parameterization of anthropogenic aerosol optical properties and an associated Twomey effect for climate studies, Geosci. Model Dev. Disc., 2016, 1–34, doi:10.5194/gmd-2016-189.

9. ARGO FLOAT DEPLOYMENTS

Birgit Klein[1] (not on board), Jan Gerken[2], Volker Strass[2]

[1]BSH
[2]AWI

Grant-No. AWI_PS113_00

Objectives

The deployment of autonomous floats in the South Atlantic Ocean represents a contribution of the Federal Republic of Germany in the context of the international Argo programme. The German contribution to the International Argo programme is organized by the Federal Maritime and Hydrographic Agency (BSH, Bundesamt für Seeschifffahrt und Hydrographie) in Hamburg. Argo is a core element of the Global Ocean Observation System (GOOS) and provides temperature and salinity profiles from the upper 2,000 m in the ocean for climate monitoring. Argo is supported by the World Meteorological Organization (WMO) and the Intergovernmental Oceanographic Commission of UNESCO (IOC). The strategy of Argo aims for an array of one float being operative in each 3°latitude x 3°longitude square of the world ocean. Floats have nominal life times of >4 years and after the battery energy supply has been depleted floats have continuously to be reseeded. Float density in the world ocean is general good, but larger gaps exist in the South Atlantic Ocean.

Work at sea

In order to fill data gaps in the South Atlantic three Argo floats were deployed along the cruise track during PS113 (Table 9.1). The float deployments were accompanied by CTD casts in support of the quality control of the float data.

Tab. 9.1: Argo float deployments

Station	Float ID	Date Time	Latitude	Longitude	CTD-Station (Depth)
PS113_3-3	AL250017DE024	11.05.2018 17:25	44° 51.411' S	056° 39.573' W	PS113_3-2 (401m)
PS113_5-3	AL250017DE025	12.05.2018 15:47	42° 10.674' S	052° 51.685' W	PS113_5-2 (398m)
PS113_10-2	AL250017DE022	16.05.2018 09:57	31° 13.761' S	039° 18.939' W	PS113_10_1 (4475m)

Data management

All floats deliver their data (vertical profiles of temperature and salinity) in near-real time to the global Argo data centers (http://www.coriolis.eu.org/Data-Products/Data-Delivery) where they are made available within 24 hours. There are no restrictions on the data use and data can be downloaded by the general public in various formats. The float data are subject to a scientific quality control in six-month intervals to identify potential problems with sensor drift. Quality controlled data are then also made available to the general public. The metadata of the scientific measurements made during PS113 have been transmitted two months after the cruise in form of the Cruise Summary Report (CSR) to the Deutsches Ozeanographisches Datenzentrum (DOD).

10. BATHYMETRY

Simon Dreutter[1], Sophie Andree[1] (embarked Las Palmas), Mona Lütjens[1] (embarked Las Palmas), Jolien van der Krogt[1] (embarked Las Palmas)

[1]AWI

Grant-No.: AWI_PS113_00

Objectives

Accurate knowledge of the seafloor topography, hence high-resolution bathymetry data, is key basic information necessary to understand many marine processes. It is of particular importance for the interpretation of scientific data in a spatial context. Bathymetry, hence geomorphology, is furthermore a basic parameter for the understanding of the general geological setting of an area and geological processes such as erosion, sediment transport and deposition. Even information on tectonic processes can be inferred from bathymetry. Supplementing the bathymetric data, high-resolution sub-bottom profiler data of the top 10s of meters below the seabed provide information on the sediments at the seafloor and on the lateral extension of sediment successions.

While world bathymetric maps give the impression of a detailed knowledge of worldwide seafloor topography, most of the world's ocean floor remains unmapped by hydroacoustic systems. In these areas, bathymetry is modelled from satellite altimetry with a corresponding low resolution. Satellite-altimetry derived bathymetry therefore lacks the resolution necessary to resolve small- to meso-scale geomorphological features (e.g. sediment waves, glaciogenic features and small seamounts). Ship-borne multibeam data provide bathymetry information in a resolution sufficient to resolve those features.

Therefore, the main task of the bathymetry group on board *Polarstern* during PS113 was to collect underway bathymetric data, including calibration and correction of the data for environmental circumstances (sound velocity, systematic errors in bottom detection, etc.), the post processing and cleaning of the data, as well as data management for on-site map creation.

Work at sea

During the PS113 cruise, the bathymetric surveys were conducted with the hull-mounted multi-beam echosounder (MBES) Atlas Hydrosweep DS3. The Hydrosweep is a deep water system for continuous mapping with the full swath potential. It operates on a frequency of ~14 kHz. On *Polarstern*, the MBES transducer arrays are arranged in a Mills cross configuration of 6 m (transmit unit) by 6 m (receive unit). The combined motion, position (Trimble GNSS), and time data comes from an iXBlue Hydrins system and the signal goes directly into the Processing Unit (PU) of the MBES to do real-time motion compensation in Pitch, Roll and Yaw. With a combination of phase and amplitude detection algorithms the PU computes the water depth from the returning backscatter signal. The system can cover a sector of up to 150° with each 75° per side.

Data acquisition was carried out throughout the entire cruise, as long as the ship was sailing in international waters. The MBES was operated with Atlas Hydromap Control and for online data visualization Teledyne PDS was used. The collected bathymetry was stored in ASD and S7K raw files. Subsequent data processing was performed using Caris HIPS and SIPS. For generating maps, the data were exported to Quantum GIS in the GeoTIFF raster format.

Preliminary results

For best survey results with correct depths, the CTD (Conductivity, Temperature, Depth) casts, performed by the oceanographic working group were used to measure the water sound velocity in the different depths. This is essential, as the acoustic signal travels down the water column from the transducer to the seafloor and back to the surface through several different layers of water masses with each a different sound velocity. The sound velocity is influenced by density and compressibility, both depending on pressure, temperature and salinity. Wrong or outdated sound velocity profiles lead to refraction errors and reduced data quality. The CTD measures conductivity, temperature, and depth in the water column while it is lowered to the seafloor. From these parameters, the sound velocity is calculated. The sound velocity profiles obtained by the CTD were immediately processed (shown in Fig. 10.1) and applied within the MBES for correct beamforming during the survey.

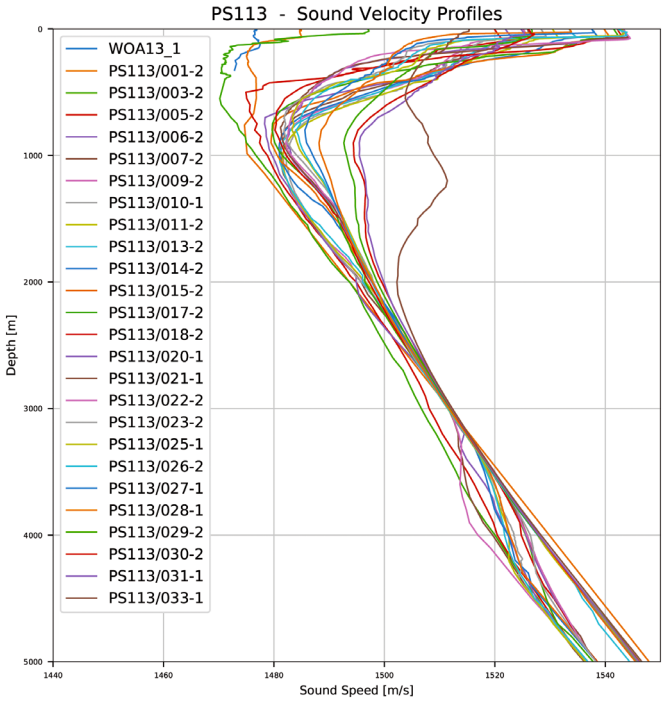

Fig. 10.1: Sound Velocity Profiles used during PS113 (all profiles are extended below the maximum depths of the CTD casts with World Ocean Atlas 2013 data and virtually extrapolated to 12,000 m water depth)

Throughout the cruise a continuous recording of data was achieved, except for small data gaps due to unexpected system/software errors and shutdowns. During 23 days of survey, a track length of 5,089 nm (9,425 km) was surveyed by the swath bathymetry system. The raw data volume of the Hydrosweep is 59 GB with 1311 separate files.

Data management

The collection of underway data during PS113 will contribute to the bathymetry data archive at the AWI and additionally contribute to bathymetric world datasets like GEBCO (General Bathymetric Chart of the Oceans). The raw datasets will be ingested to PANGAEA Data Publisher for Earth & Environmental Science. The metadata of the scientific measurements made during PS113 have been transmitted two months after the cruise in form of the Cruise Summary Report (CSR) to the Deutsches Ozeanographisches Datenzentrum (DOD).

11. CLIMATE SENSITIVITY IN VARIOUS FISHES FROM THE ANTARCTIC PENINSULA: MOLECULAR ECOLOGY AND CELLULAR MECHANISMS

Anette Tillmann[1], Bastian Maus[1], Magnus Lucassen[1] (not on board), C. Papetti[2] (not on board), Nils Koschnick[1] (not on board)

[1]AWI
[2]UniPd

Grant-No. AWI_PS113_03

Objectives

The ongoing release of the greenhouse gas CO_2 into the atmosphere is believed to cause both, global warming and ocean acidification. The changes largely differ between regions, and the Antarctic Peninsula is one area of the globe that is currently experiencing rapid warming. As solubility of CO_2 is enhanced in cold waters, the impact of climate change might be severed by the combination of both climate factors especially in the study area of the previous expedition (PS112).

Temperature as a main abiotic factor comprises every aspect of the biochemistry and physiology of ectothermal organisms putatively culminating in shifting geographical distribution on a larger scale. Although limits may become manifested at the whole organism first, all levels of organization from the genetic basement to functional physiological levels are involved. For an understanding of climate-driven evolution and response to ongoing change, the integration of molecules into functional units and networks up to the whole animal must therefore be taken into account.

To continue our comprehensive physiological and molecular genetic studies of high and low Antarctic fish species and populations, live fish in the most pristine condition possible is indispensable for our physiological work. Especially the Antarctic eelpout (*Pachycara brachycephalum*) became an ideal model for our research resulting in a reasonable number of comparative studies during the past (*cf*. Windisch et al., 2014). Moreover, endemic Notothenioids were included more recently to expand our evidences to different fish groups. During PS112 we have caught fish from several fish orders and kept them alive to bring them to the home institute for physiological analyses and genetic profiling. There, we aim to (i) estimate acclimatory capacities/sensitivity towards combined treatments of warming, hypoxia and hypercapnia, (ii) determine the level of cold adaptation, and (iii) compare those laboratory-treated samples to *in-situ* samples from the field. The analyses comprise global (RNA-Seq) and targeted (qPCR) gene expression techniques considering the genetic background and population structure, assessment of cellular energy budgets and allocation, as well as metabolic profiling (by means of untargeted nuclear magnetic resonance spectroscopy, NMR).

The response of a species to changing environmental conditions largely depends on the genetic variation within populations. The pressure of these factors on natural populations at the edges of their distribution window may affect the population structure and variance. Using transcriptomic approaches, new candidate genes, which are under selective pressure and are adaptive for cold adaptation, can be isolated. However, their selective nature can only be validated on the background of neutral genetic markers. Thus, population genetic structure

and dynamics are being assessed alongside our functional genomic approaches in all species under study (Papetti et al., 2016; 2012; Angostini et al., 2015).

At the cellular level temperature-dependent metabolic adjustments are key to maintain energetic homeostasis and thus functioning and survival of the animal at various temperatures. In the past, we examined the effect of acute warming on cellular energy metabolism in primary cell cultures of different Antarctic fish species (Mark et al., 2005). In line with the species' geographical distribution and environmental temperature exposure temperature-induced changes in cell metabolism in particular in cellular energy expenditure for protein synthesis differed between species thereby paralleling the degree of cold adaptation (Lannig et al., unpublished). According to the findings that thermal sensitivity of cell metabolism mirrors organism temperature tolerance another aim of the present project is to unravel the metabolic pathways and molecular mechanisms underlying cellular response to warming. Therefore, several fish species have been used to isolate cells for establishing permanent cell lines for later use at the home institute.

Work at sea

Monitoring and transport of life Antarctic fish

Fishes caught during the previous cruise leg PS112 were kept alive on board *Polarstern* for further studies of various physiological parameters at the home institute. In total, ~500 Antarctic eelpouts *Pachycara brachycephalum* and individual Yellow-fin rockcod *Lepidonotothen nudifrons* – derived from the fish lift (see Lucassen et al., 2018) – were kept in a circulating seawater system, at temperatures between 0-5°C. Water quality, represented by its ammonium content, was determined regularly through photometry (Nanocolor Ammonium Quicktest), and deemed sufficient at values < 0.4 mg NH_4^+ L^{-1}. To keep ammonia levels in this range, ~1 m^3 of seawater was exchanged for pre-cooled water twice a day.

Maintenance of cell cultures from Antarctic fish

Primary cell cultures were isolated from various tissues (liver, spleen kidney and head kidney) and several low- and high-Antarctic fish species during the previous cruise PS112 (*cf*. Stapp et al., 2015) to establish permanent cell lines of Antarctic fish for the first time. Therefore, carriage of the cells had to be continued on the present cruise PS113 until Bremerhaven. Cells were kept at 0°C in their respective medium. Cell condition was monitored regularly under a light microscope.

Preliminary results

Fish transport

Over the entire cruise, only 4 eelpouts died of unknown reasons. Thus, more than 99 % of the eelpouts survived. All *L. nudifrons*, which were caught by means of a bottom trawl but recovered from the fish lift, a device to protect fishes against the threat of the cod-end, survived, confirming the principal applicability of the fish lift. Future efforts are aimed at optimisation of the fish lift to increase the number of fish entering the fish lift.

Cell cultures

Due to the low temperatures, no significant growth of the cultures could be observed. The exchange of medium was reduced to once per week. Isolates prepared of liver and spleen tissue from the low-Antarctic species *Gobionothoten gibberifrons* did not survive until the end of the cruise.

From the high-Antarctic species *Trematomus bernacchii* cell cultures of kidney and spleen contained very low numbers of living cells, but liver cells did not survive. Head-kidney cells seemed to be in stable condition with both small free-swimming aggregates in the medium and a thin cell layer at the well bottom. For the third species, the high-Antarctic *Trematomus hansoni*, a very thin layer of liver cells could be observed around the center of the well bottom. Spleen, kidney and head kidney cells were mostly dead.

In summary, at least some cell cultures isolated from Antarctic fish survived since their isolation and until disembarkation in Bremerhaven for more than 3 months. These isolates will be kept alive as long as possible at the home institute for cell typing and preliminary physiological studies.

Data management

All data will be made available by publication in scientific journals and subsequent storage in in PANGAEA Data Publisher for Earth & Environmental Science. The molecular data will be submitted to the respective database (NCBI; EMBL).

References

Agostini C, Patarnello T, Ashford JR, Torres JJ, Zane L, and Papetti C (2015) Genetic differentiation in the ice-dependent fish *Pleuragramma antarctica* along the Antarctic Peninsula. Journal of Biogeography 42(6), 1103–1113.

Lucassen M, Papetti C, Koschnick N, Lannig-Bock G, Mark F, Bock C (2018) Climate Sensitivity in Various Fishes from the Antarctic Peninsula: Molecular Ecology and Cellular Mechanisms. Pp 51 - 60 in: Meyer B and Wessels W (eds) The Expedition PS112 of the Research Vessel POLARSTERN to the Antarctic Peninsula Region in 2018, Berichte zur Polar- und Meeresforschung = Reports on polar and marine research, Bremerhaven, Alfred Wegener Institute for Polar and Marine Research, 722, 125 p. doi:10.2312/BzPM_0722_2018.

Mark FC, Hirse T, and Pörtner H-O (2005) Thermal sensitivity of cellular energy budgets in Antarctic fish hepatocytes. Polar biology, 28 (11), pp. 805-814.

Papetti C, Lucassen M, and Pörtner H-O (2016) Integrated studies of organismal plasticity through physiological and transcriptomic approaches: examples from marine polar regions. Briefings in Functional Genomics, elw024. doi:10.1093/bfgp/elw024.

Stapp L, Kreiss C, Pörtner H-O, and Lannig G (2015) Differential impacts of elevated CO_2 and acidosis on the energy budget of gill and liver cells from Atlantic cod, *Gadus morhua*. Comparative Biochemistry and Physiology, Part A 187 (2015) 160–167.

Windisch HS, Frickenhaus S, John U, Knust R, Pörtner H-O, and Lucassen M (2014) Stress response or beneficial temperature acclimation: Transcriptomic signatures in Antarctic fish (*Pachycara brachycephalum*). Molecular Ecology, 23 (14), 3469-3482.

A.1 TEILNEHMENDE INSTITUTE / PARTICIPATING INSTITUTIONS

	Address
AWI	Alfred-Wegener-Institut Helmholtz-Zentrum für Polar- und Meeresforschung Postfach 120161 27515 Bremerhaven Germany
BSH	Bundesamt für Seeschifffahrt und Hydrographie Operationelle Ozeanographie Bernhard-Nocht-Str. 78 20359 Hamburg Germany
DWD	Deutscher Wetterdienst Geschäftsbereich Wettervorhersage Seeschifffahrtsberatung Bernhard Nocht Str. 76 20359 Hamburg Germany
IUP	Institut für Umweltphysik Universität Bremen Postfach 33 04 40 D-28334 Bremen Deutschland
MPI-M	Max-Planck-Institut für Meteorologie Bundesstraße 53 D-20146 Hamburg Germany
OWS	OceanWaveS GmbH Hansekontor Vor dem Bardowicker Tore 6b D-21339 Lüneburg Germany
RFL	Reederei F. Laeisz G.m.b.H. Zweigniederlassung Bremerhaven Bartelstraße 1 27570 Bremerhaven Germany

	Address
TROPOS	Leibniz-Institut für Troposphärenforschung (TROPOS) Permoserstraße 15 D-04318 Leipzig Germany
UFSC	Universidade Federal de Santa Catarina Departamento de Engenharia Mecânica Campus Universitário Reitor João David Ferreira Lima Trindade – Florianópolis SC. 88040-900 Brazil
UniPd	University of Padova Department of Biology Via U. Bassi 58/B I-35131 Padova Italy
UniHB	Universität Bremen Bibliothekstraße 1 28359 Bremen Germany
UoL	Dept. of Earth, Ocean and Ecological Sciences School of Environmental Sciences University of Liverpool 4 Brownlow Street Liverpool, L69 3GP UK

A.2 FAHRTTEILNEHMER / CRUISE PARTICIPANTS

Name/ Last name	Vorname/ First name	Institut/ Institute	Beruf/ Profession	Fachbereich/ Discipline
Andree	Sophie	AWI	Student (from Las Palmas)	Bathymetry
Bracher	Astrid	AWI	Scientist	Oceanography
Dreutter	Simon	AWI	Technician	Bathymetry
El Naggar	Saad	RFL	Scientist	Physics
Gerken	Jan	AWI	Student	Oceanography
Haake	Hauke	AWI	Engineer	Marine Technology
Hagemann	Jonas	AWI	Engineer (to Las Palmas)	Marine Technology
Hempelt	Juliane	DWD	Technician	Meteorology
Hessner	Katrin	OWS	Scientist	Oceanography
Hörstmann	Cora	AWI	Phd Student	Biology
Jimenez	Cristofer	TROPOS	Phd Student	Physics
Leach	Harry	UoL	Scientist	Oceanography
Lenius	Sven	AWI	Student	Oceanography
Lütjens	Mona	AWI	Student (from Las Palmas)	Bathymetry
Maus	Bastian	AWI	Scientist	Biology
Miller	Max	DWD	Scientist	Meteorology
Neubauer	Augusto	AWI, UFSC	Student	Engineering
Radenz	Martin	TROPOS	Phd Student	Meteorology
Spahic´	Susanne	AWI	Technician	Biology
Strass	Volker	AWI	Chief Scientist	Oceanography
Tillmann	Anette	AWI	Technician	Biology
Thomé	Pauline	AWI	Student	Biology
Vial	Jessica	MPI-M	Scientist	Environmental Sci.
Van der Krogt	Jolien	AWI	Student (from Las Palmas)	Bathymetry
Von Appen	Wilken-Jon	AWI	Scientist	Oceanography
Waite	Anya	AWI	Scientist (from Las Palmas)	Biology
Wiegmann	Sonja	AWI	Technician	Oceanography
Xi	Hongyan	AWI	Scientist	Oceanography
Yin	Zhengping	TROPOS	Phd Student	Physics

A.3 SCHIFFSBESATZUNG / SHIP'S CREW

No.	Name	First Name	Rank
1	Schwarze	Stefan	Master
2	Grundmann	Uwe	Chiefmate
3	Lauber	Felix	1st Mate
4	Fischer	Tibor	2nd Mate
5	Peine	Lutz Gerhard	2nd Mate
6	Westphal	Henning	Chief
7	Buch	Erik-Torsten	2nd Eng.
8	Rusch	Torben	2nd Eng.
9	Schnürch	Helmut	2nd Eng.
10	Brehme	Andreas	E-Eng.
11	Hofmann	Walter Jörg	ChiefELO
12	Feiertag	Thomas	ELO
13	Frank	Gerhard	ELO
14	Winter	Andreas	ELO
15	Pohl	Klaus	Ships doc
16	Sedlak	Andreas	Bosun
17	Neisner	Winfried	Carpen.
18	Clasen	Nils	MP Rat.
19	Müller	Steffen	MP Rat.
20	Schröder	Horst	MP Rat.
21	Schröder	Norbert	MP Rat.
22	Brickmann	Peter	AB
23	Fölster	Michael	AB
24	Hartwig-Labahn	Andreas	AB
25	Beth	Detlef	Storek.
26	Plehn	Markus	MP Rat
27	Waterstradt	Felix	MP Rat
28	Dinse	Horst	MM
29	Krösche	Eckard	MM
30	Watzel	Bernhard	MM
31	Meißner	Jörg	Cook
32	Lehmann	Christian	Cooksm.
33	Tupy	Mario Gottfried ...	Cooksm.
34	Wartenberg	Irina	ChiefStew.
35	Chen	Quan Lun	2nd Stew.
36	Duka	Maribel	2nd Stew.
37	Hischke	Peggy	2nd Stew.
38	Krause	Tomasz	2nd Stew.
39	Mack	Ulrich Helmuth	2nd Stew.
40	Shi	Wubo	2nd Stew.
41	Sun	Yong Sheng	Laundrym.

A.4 STATIONSLISTE /STATION LIST

Station	Date	Time	Latitude	Longitude	Depth [m]	Gear	Action
PS113_0_ Underway-1	2018-05-07	10:55	-53.12543	-70.85832		WST	profile start
PS113_0_ Underway-1	2018-06-11	4:37	53.56681	8.55504		WST	profile end
PS113_0_ Underway-2	2018-05-10	17:12	-47.67633	-60.73610	383	ADCP_150	profile start
PS113_0_ Underway-2	2018-06-01	10:00	24.17800	-19.82444	3676	ADCP_150	profile end
PS113_0_ Underway-2	2018-06-04	7:30	31.17509	-14.48654	180	ADCP_150	profile start
PS113_0_ Underway-2	2018-06-09	10:50	50.27124	-0.18956	41.1	ADCP_150	profile end
PS113_0_ Underway-3	2018-05-10	17:15	-47.67011	-60.72666	388	FBOX	profile start
PS113_0_ Underway-3	2018-06-03	2:00	27.53211	-15.53761	3574	FBOX	profile end
PS113_0_ Underway-3	2018-06-03	16:59	28.45206	-15.27227		FBOX	profile start
PS113_0_ Underway-3	2018-06-09	13:08	50.40711	0.56836	31.7	FBOX	profile end
PS113_0_ Underway-4	2018-05-10	17:15	-47.66869	-60.72452	386	PCO2_GO	profile start
PS113_0_ Underway-4	2018-06-03	2:00	27.53211	-15.53761	3574	PCO2_GO	profile end
PS113_0_ Underway-4	2018-06-03	16:59	28.45133	-15.27250		PCO2_GO	profile start
PS113_0_ Underway-4	2018-06-09	13:06	50.40522	0.55951	32	PCO2_GO	profile end
PS113_0_ Underway-5	2018-05-10	17:16	-47.66637	-60.72122	385	TSG_KEEL	profile start
PS113_0_ Underway-5	2018-06-03	2:00	27.53211	-15.53761	3574	TSG_KEEL	profile end
PS113_0_ Underway-5	2018-06-03	16:59	28.45074	-15.27269		TSG_KEEL	profile start
PS113_0_ Underway-5	2018-06-09	13:08	50.40663	0.56608	31.6	TSG_KEEL	profile end

Station	Date	Time	Latitude	Longitude	Depth [m]	Gear	Action
PS113_0_ Underway-6	2018-05-10	17:17	-47.66519	-60.71956	387	TSG_KEEL_2	profile start
PS113_0_ Underway-6	2018-06-03	2:00	27.53211	-15.53761	3574	TSG_KEEL_2	profile end
PS113_0_ Underway-6	2018-06-03	16:59	28.45023	-15.27285		TSG_KEEL_2	profile start
PS113_0_ Underway-6	2018-06-09	13:07	50.40636	0.56479	31.8	TSG_KEEL_2	profile end
PS113_0_ Underway-7	2018-05-10	17:18	-47.66282	-60.71614	388	PCO2_SUB	profile start
PS113_0_ Underway-7	2018-06-03	2:00	27.53211	-15.53761	3574	PCO2_SUB	profile end
PS113_0_ Underway-7	2018-06-03	16:58	28.44956	-15.27306		PCO2_SUB	profile start
PS113_0_ Underway-7	2018-06-09	13:07	50.40599	0.56307	31.9	PCO2_SUB	profile end
PS113_0_ Underway-8	2018-05-10	18:52	-47.63455	-60.70180	405	HSPS	profile start
PS113_0_ Underway-8	2018-06-02	10:00	26.07062	-17.58135	3560	HSPS	profile end
PS113_0_ Underway-8	2018-06-04	9:00	31.45956	-14.40733	180	HSPS	profile start
PS113_0_ Underway-8	2018-06-08	16:50	48.71339	-5.66996	115	HSPS	profile end
PS113_0_ Underway-9	2018-05-14	14:41	-35.79384	-44.78955	4847	MAG	profile start
PS113_0_ Underway-9	2018-06-11	4:37	53.56681	8.55504		MAG	profile end
PS113_0_ Underway-10	2018-05-14	14:42	-35.79387	-44.78952	4846	GRAV	profile start
PS113_0_ Underway-10	2018-06-11	4:37	53.56681	8.55504		GRAV	profile end
PS113_1-1	2018-05-10	17:26	-47.65788	-60.71668	388	SPR	station start
PS113_1-1	2018-05-10	17:50	-47.65449	-60.71628	391	SPR	at depth
PS113_1-1	2018-05-10	18:01	-47.65242	-60.71521	391	SPR	station end
PS113_1-2	2018-05-10	18:10	-47.65078	-60.71433	391	CTD	station start
PS113_1-2	2018-05-10	18:26	-47.64793	-60.71310	393	CTD	at depth
PS113_1-2	2018-05-10	18:39	-47.64558	-60.71200	389	CTD	station end

Station	Date	Time	Latitude	Longitude	Depth [m]	Gear	Action
PS113_2-1	2018-05-11	11:59	-45.09830	-57.00901	4693	topAWI	station start
PS113_2-1	2018-05-11	12:55	-44.99910	-56.86908	4861	topAWI	at depth
PS113_2-1	2018-05-11	14:09	-44.91157	-56.74592	5015	topAWI	station end
PS113_3-1	2018-05-11	14:40	-44.89889	-56.75290	5005	SPR	station start
PS113_3-1	2018-05-11	15:03	-44.89724	-56.75775	4999	SPR	at depth
PS113_3-1	2018-05-11	15:15	-44.89712	-56.75926	4998	SPR	station end
PS113_3-2	2018-05-11	15:21	-44.89712	-56.75999	4999	CTD	station start
PS113_3-2	2018-05-11	15:34	-44.89723	-56.76115	4999	CTD	at depth
PS113_3-2	2018-05-11	15:48	-44.89752	-56.76196	5001	CTD	station end
PS113_3-3	2018-05-11	17:25	-44.85685	-56.65955	5087	FLOAT	station start
PS113_4-1	2018-05-11	17:56	-44.81456	-56.59619	5138	topAWI	station start
PS113_4-1	2018-05-11	21:38	-44.50874	-56.15957	5191	topAWI	station end
PS113_5-1	2018-05-12	14:37	-42.10918	-52.87399	5619	SPR	station start
PS113_5-1	2018-05-12	14:58	-42.13020	-52.87005	5627	SPR	at depth
PS113_5-1	2018-05-12	15:03	-42.13409	-52.86922	5623	SPR	station end
PS113_5-2	2018-05-12	15:10	-42.14210	-52.86757	5671	CTD	station start
PS113_5-2	2018-05-12	15:25	-42.15537	-52.86322	5626	CTD	at depth
PS113_5-2	2018-05-12	15:40	-42.17011	-52.85866	5631	CTD	station end
PS113_5-3	2018-05-12	15:47	-42.17790	-52.86141	5632	FLOAT	station start
PS113_6-1	2018-05-13	14:32	-38.87095	-48.64552	5340	SPR	station start
PS113_6-1	2018-05-13	14:59	-38.87559	-48.64779	5291	SPR	at depth
PS113_6-1	2018-05-13	15:03	-38.87593	-48.64824	5293	SPR	station end
PS113_6-2	2018-05-13	15:14	-38.87631	-48.64934	5291	CTD	station start
PS113_6-2	2018-05-13	15:27	-38.87716	-48.64979	5293	CTD	at depth
PS113_6-2	2018-05-13	15:41	-38.87865	-48.65025	5291	CTD	station end
PS113_7-1	2018-05-14	14:37	-35.79302	-44.78977	4846	SPR	station start
PS113_7-1	2018-05-14	15:22	-35.79108	-44.78427	4843	SPR	at depth
PS113_7-1	2018-05-14	15:32	-35.79019	-44.78275	4843	SPR	station end
PS113_7-2	2018-05-14	15:43	-35.78935	-44.78102	4865	CTD	station start
PS113_7-2	2018-05-14	15:54	-35.78892	-44.77927	4865	CTD	at depth
PS113_7-2	2018-05-14	16:07	-35.78921	-44.77873	4867	CTD	station end
PS113_8-1	2018-05-14	17:20	-35.64447	-44.62799	4854	topAWI	station start
PS113_8-1	2018-05-14	21:06	-35.31104	-44.21973	4868	topAWI	station end

Station	Date	Time	Latitude	Longitude	Depth [m]	Gear	Action
PS113_9-1	2018-05-15	13:29	-33.11881	-41.58228	4571	SPR	station start
PS113_9-1	2018-05-15	14:18	-33.12192	-41.58780	4621	SPR	at depth
PS113_9-1	2018-05-15	14:31	-33.12039	-41.58925	4573	SPR	station end
PS113_9-2	2018-05-15	14:40	-33.11918	-41.59036	4571	CTD	station start
PS113_9-2	2018-05-15	14:53	-33.11730	-41.59263	4572	CTD	at depth
PS113_9-2	2018-05-15	15:10	-33.11834	-41.59395	4571	CTD	station end
PS113_10-1	2018-05-16	6:29	-31.19836	-39.31851	n.a.	CTD	station start
PS113_10-1	2018-05-16	7:56	-31.20810	-39.31570	4543	CTD	at depth
PS113_10-1	2018-05-16	9:50	-31.22998	-39.31475	4583	CTD	station end
PS113_10-2	2018-05-16	9:57	-31.22935	-39.31565	4584	FLOAT	deployed
PS113_11-1	2018-05-16	13:31	-30.66443	-39.05351	4134	SPR	station start
PS113_11-1	2018-05-16	14:23	-30.67917	-39.04418	4136	SPR	at depth
PS113_11-1	2018-05-16	14:31	-30.68124	-39.04197	4136	SPR	station end
PS113_11-2	2018-05-16	14:40	-30.68342	-39.03987	4136	CTD	station start
PS113_11-2	2018-05-16	14:53	-30.68677	-39.03766	4137	CTD	at depth
PS113_11-2	2018-05-16	15:07	-30.68944	-39.03711	4142	CTD	station end
PS113_12-1	2018-05-16	16:08	-30.55376	-38.97564	4164	topAWI	station start
PS113_12-1	2018-05-16	19:19	-30.21082	-38.82504	4214	topAWI	station end
PS113_13-1	2018-05-17	13:28	-27.05099	-37.27060	4579	SPR	station start
PS113_13-1	2018-05-17	14:03	-27.05618	-37.26668	4610	SPR	at depth
PS113_13-1	2018-05-17	14:08	-27.05730	-37.26632	4583	SPR	station end
PS113_13-2	2018-05-17	14:16	-27.05947	-37.26585	4610	CTD	station start
PS113_13-2	2018-05-17	14:29	-27.06243	-37.26490	4583	CTD	at depth
PS113_13-2	2018-05-17	14:42	-27.06443	-37.26323	4579	CTD	station end
PS113_14-1	2018-05-18	13:30	-22.98408	-35.33039	4219	SPR	station start
PS113_14-1	2018-05-18	14:11	-22.98855	-35.33435	4219	SPR	at depth
PS113_14-1	2018-05-18	14:35	-22.99100	-35.33713	4215	SPR	station end
PS113_14-2	2018-05-18	14:41	-22.99153	-35.33763	4218	CTD	station start
PS113_14-2	2018-05-18	14:54	-22.99253	-35.33919	4213	CTD	at depth
PS113_14-2	2018-05-18	15:08	-22.99370	-35.34098	4215	CTD	station end
PS113_15-1	2018-05-19	11:15	-19.59900	-33.61500	4201	CTD	station start
PS113_15-1	2018-05-19	11:29	-19.59785	-33.61522	4163	CTD	at depth
PS113_15-1	2018-05-19	11:45	-19.59660	-33.61609	4165	CTD	station end

Station	Date	Time	Latitude	Longitude	Depth [m]	Gear	Action
PS113_15-2	2018-05-19	11:56	-19.59559	-33.61700	4163	SPR	station start
PS113_15-2	2018-05-19	12:29	-19.59338	-33.62094	4165	SPR	at depth
PS113_15-2	2018-05-19	12:36	-19.59329	-33.62171	4198	SPR	station end
PS113_16-1	2018-05-19	13:38	-19.46250	-33.53806	4144	topAWI	station start
PS113_16-1	2018-05-19	18:08	-19.00961	-33.27747	4285	topAWI	station end
PS113_17-1	2018-05-20	13:32	-15.94388	-31.54328	4706	SPR	station start
PS113_17-1	2018-05-20	14:12	-15.94029	-31.54865	4745	SPR	at depth
PS113_17-1	2018-05-20	14:22	-15.93941	-31.55148	4747	SPR	station end
PS113_17-2	2018-05-20	14:34	-15.93981	-31.55396	4743	CTD	station start
PS113_17-2	2018-05-20	14:49	-15.94107	-31.55685	4737	CTD	at depth
PS113_17-2	2018-05-20	14:59	-15.94110	-31.55797	4734	CTD	station end
PS113_18-1	2018-05-21	12:31	-12.52535	-29.63516	5498	SPR	station start
PS113_18-1	2018-05-21	13:12	-12.52572	-29.63571	5528	SPR	station end
PS113_18-2	2018-05-21	13:21	-12.52576	-29.63595	5530	CTD	station start
PS113_18-2	2018-05-21	13:36	-12.52586	-29.63660	5531	CTD	at depth
PS113_18-2	2018-05-21	13:49	-12.52623	-29.63748	5527	CTD	station end
PS113_19-1	2018-05-21	14:07	-12.50964	-29.62765	5531	topAWI	station start
PS113_19-1	2018-05-21	18:01	-12.28904	-29.50847	5542	topAWI	station end
PS113_20-1	2018-05-22	9:08	-9.77637	-28.12440	5655	CTD	station start
PS113_20-1	2018-05-22	9:26	-9.77558	-28.12337	5657	CTD	at depth
PS113_20-1	2018-05-22	9:54	-9.77481	-28.12276	5652	CTD	station end
PS113_20-2	2018-05-22	10:15	-9.77118	-28.11446	5654	topAWI	station start
PS113_21-1	2018-05-22	18:22	-9.17788	-27.80054	5686	CTD	at depth
PS113_20-2	2018-05-22	18:14	-9.17964	-27.80114	5685	topAWI	station end
PS113_21-1	2018-05-22	18:27	-9.17765	-27.80122	5685	CTD	station start
PS113_21-1	2018-05-22	19:20	-9.17808	-27.79829	5685	CTD	station end
PS113_22-1	2018-05-23	11:31	-6.29421	-26.56826	5704	SPR	station start
PS113_22-1	2018-05-23	12:29	-6.28517	-26.58768	5679	SPR	station end
PS113_22-2	2018-05-23	12:47	-6.27955	-26.58964	5679	CTD	station start
PS113_22-2	2018-05-23	12:59	-6.27817	-26.59102	5683	CTD	at depth
PS113_22-2	2018-05-23	13:13	-6.27673	-26.59278	5685	CTD	station end
PS113_23-1	2018-05-24	12:19	-2.24144	-25.00890	4657	SPR	station start
PS113_23-1	2018-05-24	12:55	-2.23617	-25.02525	4624	SPR	at depth

Station	Date	Time	Latitude	Longitude	Depth [m]	Gear	Action
PS113_23-1	2018-05-24	13:06	-2.23299	-25.02991	4591	SPR	station end
PS113_23-2	2018-05-24	13:11	-2.23189	-25.03050	4587	CTD	station start
PS113_23-2	2018-05-24	13:24	-2.22984	-25.03299	4611	CTD	at depth
PS113_23-2	2018-05-24	13:38	-2.22983	-25.03561	4576	CTD	station end
PS113_24-1	2018-05-24	14:10	-2.20879	-25.02850	4576	topAWI	station start
PS113_24-1	2018-05-25	22:41	2.13040	-24.98054	3970	topAWI	station end
PS113_25-1	2018-05-25	22:58	2.13588	-24.97749	n.a.	CTD	station start
PS113_25-1	2018-05-25	23:15	2.13902	-24.98279	n.a.	CTD	at depth
PS113_25-1	2018-05-25	23:30	2.13972	-24.98512	n.a.	CTD	station end
PS113_26-1	2018-05-26	11:05	4.15726	-24.63705	4612	SPR	station start
PS113_26-1	2018-05-26	11:40	4.16281	-24.63621	4609	SPR	at depth
PS113_26-1	2018-05-26	11:50	4.16443	-24.63578	4612	SPR	station end
PS113_26-2	2018-05-26	12:01	4.16578	-24.63529	4613	CTD	station start
PS113_26-2	2018-05-26	12:13	4.16852	-24.63491	4613	CTD	at depth
PS113_26-2	2018-05-26	12:26	4.17036	-24.63366	4612	CTD	station end
PS113_27-1	2018-05-27	10:04	8.29529	-23.52508	4896	CTD	station start
PS113_27-1	2018-05-27	10:16	8.29628	-23.52504	4898	CTD	at depth
PS113_27-1	2018-05-27	10:30	8.29731	-23.52414	4897	CTD	station end
PS113_27-2	2018-05-27	10:41	8.29911	-23.52334	4897	SPR	station start
PS113_27-2	2018-05-27	11:21	8.30038	-23.52377	4860	SPR	at depth
PS113_27-2	2018-05-27	11:31	8.30097	-23.52391	4860	SPR	station end
PS113_27-3	2018-05-27	11:40	8.30149	-23.52414	4859	topAWI	station start
PS113_27-3	2018-05-27	18:25	9.09968	-23.29451	4348	topAWI	station end
PS113_28-1	2018-05-28	9:02	11.19097	-22.69255	5109	CTD	station start
PS113_28-1	2018-05-28	9:15	11.19124	-22.69401	5106	CTD	at depth
PS113_28-1	2018-05-28	9:28	11.19183	-22.69548	5109	CTD	station end
PS113_28-2	2018-05-28	9:40	11.19154	-22.69644	5111	SPR	station start
PS113_28-2	2018-05-28	10:15	11.19261	-22.70014	5108	SPR	at depth
PS113_28-2	2018-05-28	10:27	11.19360	-22.70170	5106	SPR	station end
PS113_28-3	2018-05-28	10:40	11.20032	-22.70108	5105	topAWI	station start
PS113_28-3	2018-05-28	17:40	12.21105	-22.40260	4955	topAWI	station end
PS113_29-1	2018-05-30	15:58	19.81605	-21.14802	3676	SPR	station start
PS113_29-1	2018-05-30	16:30	19.80784	-21.14817	3670	SPR	at depth

Station	Date	Time	Latitude	Longitude	Depth [m]	Gear	Action
PS113_29-1	2018-05-30	16:44	19.80495	-21.14756	3667	SPR	station end
PS113_29-2	2018-05-30	16:54	19.80465	-21.15077	3666	CTD	station start
PS113_29-2	2018-05-30	17:07	19.80400	-21.15249	3664	CTD	at depth
PS113_29-2	2018-05-30	17:22	19.80475	-21.15446	3664	CTD	station end
PS113_29-3	2018-05-30	17:33	19.80722	-21.14615	3669	topAWI	station start
PS113_29-3	2018-05-31	16:25	22.60713	-20.52879	4159	topAWI	station end
PS113_30-1	2018-05-31	16:40	22.60815	-20.53547	4217	SPR	station start
PS113_30-1	2018-05-31	17:18	22.60773	-20.54006	4219	SPR	at depth
PS113_30-1	2018-05-31	17:28	22.60792	-20.54072	4216	SPR	station end
PS113_30-2	2018-05-31	17:38	22.61010	-20.54432	4222	CTD	station start
PS113_30-2	2018-05-31	17:52	22.61232	-20.54598	4221	CTD	at depth
PS113_30-2	2018-05-31	18:05	22.61376	-20.54749	4219	CTD	station end
PS113_31-1	2018-06-01	8:04	24.15531	-19.80369	3657	CTD	station start
PS113_31-1	2018-06-01	8:19	24.15580	-19.80525	3657	CTD	at depth
PS113_31-1	2018-06-01	8:38	24.15706	-19.80788	3660	CTD	station end
PS113_31-2	2018-06-01	8:38	24.15707	-19.80791	3662	SPR	station start
PS113_31-2	2018-06-01	9:29	24.16300	-19.81248	3664	SPR	at depth
PS113_31-2	2018-06-01	9:38	24.16468	-19.81314	3666	SPR	station end
PS113_31-3	2018-06-01	9:55	24.17156	-19.82393	3678	topAWI	station start
PS113_31-3	2018-06-01	16:55	24.73035	-19.43203	3337	topAWI	station end
PS113_32-1	2018-06-05	5:35	35.36355	-13.29334	4846	topAWI	station start
PS113_32-1	2018-06-05	10:17	35.95315	-13.11570	4847	topAWI	station end
PS113_33-1	2018-06-05	10:32	35.95687	-13.11799	4846	CTD	station start
PS113_33-1	2018-06-05	10:40	35.95634	-13.11880	4845	CTD	at depth
PS113_33-1	2018-06-05	10:50	35.95584	-13.11991	4849	CTD	station end
PS113_33-2	2018-06-05	11:00	35.95553	-13.12188	4846	SPR	station start
PS113_33-2	2018-06-05	11:44	35.94944	-13.12105	4843	SPR	at depth
PS113_33-2	2018-06-05	11:56	35.94900	-13.12195	4847	SPR	station end

Gear abbreviations	Gear
ADCP_150	ADCP 150kHz
CTD	CTD aboard RV Polarstern
FBOX	FerryBox
FLOAT	Float
GRAV	Sea Gravimeter
HSPS	Hydrosweep-Parasound
MAG	Magnetometer
PCO2_GO	pCO2 GO
PCO2_SUB	pCO2 Subctech
SPR	RAMSES
TSG_KEEL	Thermosalinograph Keel
TSG_KEEL_2	Thermosalinograph Keel 2
WST	Weatherstation
topAWI	Triaxus Towing System
WST	Weatherstation

Die **Berichte zur Polar- und Meeresforschung** (ISSN 1866-3192) werden beginnend mit dem Band 569 (2008) als Open-Access-Publikation herausgegeben. Ein Verzeichnis aller Bände einschließlich der Druckausgaben (ISSN 1618-3193, Band 377-568, von 2000 bis 2008) sowie der früheren **Berichte zur Polarforschung** (ISSN 0176-5027, Band 1-376, von 1981 bis 2000) befindet sich im electronic Publication Information Center **(ePIC)** des Alfred-Wegener-Instituts, Helmholtz-Zentrum für Polar- und Meeresforschung (AWI); see http://epic.awi.de. Durch Auswahl “Reports on Polar- and Marine Research“ (via “browse”/”type”) wird eine Liste der Publikationen, sortiert nach Bandnummer, innerhalb der absteigenden chronologischen Reihenfolge der Jahrgänge mit Verweis auf das jeweilige pdf-Symbol zum Herunterladen angezeigt.

The **Reports on Polar and Marine Research** (ISSN 1866-3192) are available as open access publications since 2008. A table of all volumes including the printed issues (ISSN 1618-3193, Vol. 377-568, from 2000 until 2008), as well as the earlier **Reports on Polar Research** (ISSN 0176-5027, Vol. 1-376, from 1981 until 2000) is provided by the electronic Publication Information Center **(ePIC)** of the Alfred Wegener Institute, Helmholtz Centre for Polar and Marine Research (AWI); see URL http://epic.awi.de. To generate a list of all Reports, use the URL http://epic.awi.de and select “browse”/ ”type” to browse ”Reports on Polar and Marine Research”. A chronological list in declining order will be presented, and pdf-icons displayed for downloading.

Zuletzt erschienene Ausgaben:

Recently published issues:

724 (2018) The Expedition PS113 of the Research Vessel POLARSTERN to the Atlantic Ocean in 2018, edited by Volker Strass

723 (2018) The Expedition PS114 of the Research Vessel POLARSTERN to the Fram Strait in 2018, edited by Wilken-Jon von Appen

722 (2018) The Expedition PS112 of the Research Vessel POLARSTERN to the Antarctic Peninsula Region in 2018, edited by Bettina Meyer and Wiebke Weßels

721 (2018) Alfred Wegener im 1. Weltkrieg. Ein Polarforscher und die „Urkatastrophe des 20. Jahrhunderts“, by Christian R. Salewski

720 (2018) The Expedition PS98 of the Research Vessel POLARSTERN to the Atlantic Ocean in 2016, edited by Bernhard Pospichal

719 (2018) The Expeditions PS106/1 and 2 of the Research Vessel POLARSTERN to the Arctic Ocean in 2017, edited by Andreas Macke and Hauke Flores

718 (2018) The Expedition PS111 of the Research Vessel POLARSTERN to the southern Weddell Sea in 2018, edited by Michael Schröder

717 (2018) The Expedition PS107 of the Research Vessel POLARSTERN to the Fram Strait and the AWI-HAUSGARTEN in 2017, edited by Ingo Schewe

716 (2018) Polar Systems under Pressure, 27th International Polar Conference, Rostock, 25 - 29 March 2018, German Society for Polar Research, edited by H. Kassens, D. Damaske, B. Diekmann, D. Fütterer, G. Heinemann, U. Karsten, E.M. Pfeiffer, J. Regnery, M. Scheinert, J. Thiede, R. Tiedemann & D. Wagner

715 (2018) The Expedition PS109 of the Research Vessel POLARSTERN to the Nordic Seas in 2017, edited by Torsten Kanzow

714 (2017) The Expedition SO258/2 of the Research Vessel SONNE to the central Indian Ocean in 2017, edited by Wolfram Geissler

ALFRED-WEGENER-INSTITUT
HELMHOLTZ-ZENTRUM FÜR POLAR-
UND MEERESFORSCHUNG

BREMERHAVEN

Am Handelshafen 12
27570 Bremerhaven
Telefon 0471 4831-0
Telefax 0471 4831-1149
www.awi.de

HELMHOLTZ
GEMEINSCHAFT